

1 **Title: A mechanism for hippocampal memory recall based on excitatory-inhibitory**  
2 **fluctuations in neocortex**

3  
4 **Authors:** Renée S. Koolschijn<sup>1†\*</sup>, Anna Shpektor<sup>1†</sup>, I. Betina Ip<sup>1,2</sup>, William T. Clarke<sup>1</sup>, David  
5 Dupret<sup>3</sup>, Uzay E. Emir<sup>1,4</sup>, Helen C. Barron<sup>1,3\*</sup>

6  
7 \* Corresponding authors

8 † indicates equal contribution

9

10 **Author affiliations:**

11 1. Wellcome Centre for Integrative Neuroimaging, University of Oxford, FMRIB, John  
12 Radcliffe Hospital, Oxford, OX3 9DU, UK. 2. Department of Physiology, Anatomy and  
13 Genetics, University of Oxford OX1 3PT, UK. 3. Medical Research Council Brain Network  
14 Dynamics Unit, University of Oxford, Mansfield Road, Oxford, OX1 3TH, UK. 4. School of  
15 Health Sciences, Purdue University, IN 47907, USA.

16

17 **Contact:**

18 Corresponding authors: Renée Koolschijn ([renee.koolschijn@keble.ox.ac.uk](mailto:renee.koolschijn@keble.ox.ac.uk)) and Helen  
19 Barron ([helen.barron@merton.ox.ac.uk](mailto:helen.barron@merton.ox.ac.uk))

20 **ABSTRACT**

21 The brain has a remarkable capacity to acquire and store memories that can later be selectively  
22 recalled. These processes are supported by the hippocampus which is thought to index memory  
23 recall by reinstating information stored across distributed neocortical circuits. However, the  
24 mechanism that supports this interaction remains unclear. Here, in humans, we show that recall  
25 of a visual cue from a paired associate is accompanied by a transient increase in the ratio  
26 between glutamate and GABA in visual cortex. Moreover, these excitatory-inhibitory  
27 fluctuations are predicted by activity in the hippocampus. These data suggest the hippocampus  
28 gates memory recall by indexing information stored across neocortical circuits using a  
29 disinhibitory mechanism.

30

31 **INTRODUCTION**

32 Memories are thought to be stored across sparse and distributed neuronal ensembles in the  
33 brain<sup>1,2</sup>. To facilitate memory recall, activity across neuronal ensembles is selectively  
34 reinstated to recover enduring representations of the past. This reinstatement is thought to be  
35 mediated by the hippocampus, a brain region important for learning and memory<sup>3</sup>.  
36 Anatomically, the hippocampus sits at the apex of a cortical sensory processing hierarchy<sup>4</sup>  
37 where inputs received by sensory cortices reach the hippocampus via the entorhinal cortex and  
38 other relay regions, which in turn make widespread cortico-cortical connections that project  
39 the hippocampal output back to neocortex<sup>5,6</sup>. This reciprocal anatomical connectivity equips  
40 the hippocampus with the necessary architecture to coordinate activity with neocortex, thus  
41 providing a ‘memory index’, or summary sketch, for information stored across distributed  
42 cortical circuits<sup>7-9</sup>. Consistent with this view, during memory recall hippocampal reinstatement  
43 predicts subsequent neocortical reinstatement<sup>10</sup>.

44

45 However, the mechanism that allows the hippocampus to coordinate reinstatement across  
46 distributed neocortical circuits remains unclear. In animal models, neural circuit manipulations  
47 suggest higher-order brain regions may modulate release of sensory information in neocortex  
48 via disinhibitory circuit mechanisms<sup>11,12</sup>. For example, during attentional modulation,  
49 projections from the cingulate region of mouse frontal cortex modulate GABAergic circuits in  
50 visual cortex to enhance visual discrimination<sup>13</sup>. Building upon this idea, one possibility is that  
51 the hippocampus mediates memory recall using a similar mechanism, by transiently  
52 modulating the relationship between neocortical excitation and inhibition.

53

54 At the cellular level, tight coupling between neocortical excitation and inhibition (EI) can be  
55 observed during both sensory stimulation and spontaneous neural activity<sup>14-16</sup>. This  
56 phenomenon has led to the concept of EI balance, where, following changes in excitability,  
57 synaptic strength, current or overall network activity returns to a stable set point via negative  
58 feedback<sup>17</sup>. Therefore, while microcircuits are capable of large changes in activity due to  
59 synaptic delays or differences in signal propagation speed, transient excitatory responses are  
60 rapidly quenched by inhibition<sup>16,18</sup>. The dynamic interplay between excitation and inhibition  
61 may therefore shape computations performed by cortical circuits, including in response to  
62 inputs that derive from brain regions such as the hippocampus.

63

64 While physiological measures of EI balance vary in both definition and granularity, non-  
65 invasive methods available for imaging the human brain are acquired at a more coarse  
66 spatiotemporal scale. Magnetic Resonance Spectroscopy (MRS) provides a unique tool to  
67 quantify the concentration of different neural metabolites<sup>19,20</sup>, including glutamate and GABA,  
68 the principle excitatory and inhibitory neurotransmitters in the brain. While MRS cannot  
69 dissociate between neurotransmitter and metabolic pools of glutamate and GABA<sup>21,22</sup>,  
70 meaningful interpretation of MRS-derived measures derives from a major body of work  
71 showing an approximately 1:1 relationship between the rate of glutamine-glutamate cycling,  
72 which is necessary for glutamate and GABA synthesis, and neuronal oxidative glucose  
73 consumption, which indirectly supports neurotransmitter release among other processes<sup>23-25</sup>.  
74 Moreover, despite providing an indirect measure, MRS-derived glutamate and GABA reported  
75 during learning and memory paradigms in humans show remarkable correspondence with  
76 findings reported at the physiological level in animals. For example, in animals a reduction in  
77 GABAergic tone is necessary for induction of neocortical plasticity via long-term potentiation  
78 (LTP)<sup>26,27</sup>, while in humans motor learning and plasticity in visual cortex are accompanied by  
79 a reduction in MRS-derived GABA<sup>28,29</sup>. Investigations in both animal models and humans  
80 further show that after new learning EI balance prevails to ensure memories are stored in a  
81 stable and dormant state<sup>30-32</sup>. This leads to the following prediction: memory recall involves a  
82 transient break in EI balance, opening a window to release memories from the blanket of  
83 inhibition before re-establishing network stability. Moreover, MRS-derived measures of  
84 glutamate and GABA may provide a suitable index for this process.

85

86 To test this prediction, here we implement a new sequence that combines functional Magnetic  
87 Resonance Imaging (fMRI) with functional MRS (fMRS). Together with an event-related

88 design, we use the Blood-Oxygen-Level-Dependent (BOLD) signal to probe hippocampal-  
89 dependent associative memory recall of a visual cue, while simultaneously measuring dynamic  
90 changes in MRS-derived glutamate and GABA in visual cortex. During memory recall, we  
91 report a transient increase in the ratio between MRS-derived glutamate and GABA in neocortex  
92 which is selectively predicted by the BOLD signal in the hippocampus. These findings suggest  
93 the hippocampus indexes recall by transiently modulating neocortical EI balance to release  
94 memories stored across distributed neural circuits.

95

## 96 **RESULTS**

### 97 **Task design and behaviour**

98 To investigate the neuronal mechanisms that support memory recall we designed a three-stage  
99 inference task (Fig. 1a) that has previously been shown to involve associative memory recall  
100 in humans and mice<sup>33</sup>. Moreover, we chose to implement an inference task because, unlike  
101 some forms of first-order associative recall, previous lesion and optogenetic studies in rodents  
102 demonstrate that second-order associative recall required for inference is a hippocampal  
103 dependent process<sup>33-35</sup>. Thus, the inference task provided an opportunity to investigate how the  
104 hippocampus mediates neocortical excitation and inhibition during memory recall.

105

106 In the first stage of the task participants learned up to 80 auditory-visual associations  
107 ('observational learning', day 1; Fig. 1a, Supplementary Fig. 1). In the second stage, which  
108 occurred approximately 24 hours later, each visual cue was paired with either a rewarding (set  
109 1) or neutral outcome (set 2) ('conditioning', day 2; Fig. 1a, Supplementary Fig. 1). Rewarding  
110 outcomes were silver coins that were later exchangeable for a monetary sum, while neutral  
111 outcomes were non-exchangeable woodchips. Importantly, auditory cues were never paired  
112 with an outcome, providing an opportunity to assess evidence for an inferred relationship  
113 between these indirectly related stimuli. Accordingly, in the third stage of the task we presented  
114 auditory cues in isolation, without visual cues or outcomes, and we measured evidence for  
115 inference from the auditory cues to the appropriate outcome ('inference test', day 3; Fig. 1a).  
116 All stages of the task, including the day 3 inference test were performed in virtual reality (VR)  
117 (Fig. 1b), an immersive and highly controlled 3D environment that has the potential to benefit  
118 from cross-species comparisons in the future<sup>33</sup>.

119

120 Participants performed the day 3 inference test during an MRI scan (Fig. 1c-d). In response to  
121 the auditory cues in the inference test, participants successfully inferred the correct outcome if

122 they could later recall the relevant auditory-visual association during a surprise post-scan  
123 associative memory test performed after the inference task was completed (Fig. 1e-g). Indeed,  
124 performance on the associative memory test, that assessed memory for auditory-visual  
125 associations learned on day 1, predicted performance on the inference test performed on day 3  
126 (Fig. 1h). Consistent with previous neuroimaging data in humans and cellular recordings in  
127 mice<sup>33</sup>, these behavioural findings suggest inferential choice during the inference test involves  
128 associative recall of the intermediary visual cues. In this manner, the inference task provides a  
129 suitable paradigm to investigate the neural mechanisms that underlie hippocampal-dependent  
130 associative memory recall.

131

### 132 **BOLD signal in the hippocampus and visual cortex is modulated during memory recall**

133 To investigate the relationship between the hippocampus and neocortex during associative  
134 memory recall we implemented a novel imaging sequence<sup>36</sup>, which enabled interleaved  
135 acquisition of near-whole brain fMRI together with fMRS in V1 (Fig. 2a). This imaging  
136 sequence thus provided a means to simultaneously measure both hemodynamic and  
137 neurochemical changes during the inference task, in an event-related manner.

138

139 Using fMRI data from the interleaved sequence, we first identified brain regions modulated by  
140 recall of a visual cue in response to the associated auditory cue presented during the inference  
141 test (Fig. 1a). To obtain the most accurate estimate for associative memory recall, we  
142 categorized trials post-hoc, using participants' behavioural performance from both the  
143 inference test and subsequent post-scan associative memory test (Fig. 1c-e), which were highly  
144 correlated across participants (Fig. 1h). Trials where participants made both the correct  
145 inference and subsequently remembered the auditory-visual associations were classified as  
146 'remembered'. Trials where participants made either the incorrect inference or subsequently  
147 forgot the auditory-visual associations were classified as 'forgotten' (Fig. 2b, Supplementary  
148 Table 2, *Methods*). Neural signatures acquired during the 'forgotten' trials thus provided a  
149 control condition for those acquired during the 'remembered' trials. Consistent with previous  
150 research investigating associative recall of visual cues<sup>37,38</sup>, we observed a significant increase  
151 in BOLD signal in both the hippocampus and visual cortex on 'remembered' versus 'forgotten'  
152 trials (Fig. 2c; Supplementary Fig. 2).

153

154 **Dynamic increase in the ratio between glutamate and GABA in visual cortex during recall**

155 We then asked whether associative memory recall of a visual cue is also accompanied by  
156 changes in the ratio between glutamate and GABA ('glu/GABA ratio') in the visual cortex.  
157 Using the interleaved fMRS data acquired in primary visual cortex (V1) (Fig. 2a,d), we  
158 quantified the concentration of glutamate and GABA normalised to total Creatine (tCr) in an  
159 event-related manner (Fig. 2b,e). We then used MRS-derived measures of glutamate and  
160 GABA to estimate changes in glu/GABA ratio<sup>39</sup> (see *Methods*), where changes are evaluated  
161 through assessment of the ratio of 'remembered' trials relative to 'forgotten' (as defined  
162 above). In this manner, the 'forgotten' trials again provide a condition and stimulus-matched  
163 control for data acquired during the 'remembered' trials.

164  
165 To detect dynamic changes in glu/GABA ratio it was not appropriate to implement default  
166 assumptions typically used to detect static estimates (see *Methods*). Namely, these default  
167 assumptions assume the dynamic range of GABA is fixed by normalising GABA relative to  
168 other more abundant metabolites. Here, to optimise our sensitivity to changes in glu/GABA  
169 across conditions we removed these default constraints. Notably, while this approach leads to  
170 higher GABA estimates, the uncertainty in the metabolite estimates were reduced  
171 (Supplementary Fig. 3). Moreover, our analysis controlled for any effect of metabolite scaling  
172 by comparing the difference between two conditions ('remembered' versus 'forgotten').

173  
174 During recall, we observed an increase in glu/GABA ratio in V1 when comparing  
175 'remembered' versus 'forgotten' cues (Fig. 3a-b). Standard quality metrics indicated that our  
176 data quality was comparable with those reported in previous studies<sup>40-43</sup> (Supplementary Fig.  
177 4, Supplementary Table 4). To control for any biases introduced by differences in the number  
178 of 'remembered' versus 'forgotten' trials (Supplementary Table 5), we compared the group  
179 mean metabolite change against a null distribution generated by permuting the identity labels  
180 assigned to each trial. This analysis revealed a significant decrease in GABA and a significant  
181 increase in glu/GABA ratio during memory recall (Fig. 3d-f). This change in glu/GABA ratio  
182 was still observed when using performance on the inference task alone to categorise trials into  
183 'remembered' and 'forgotten' (Supplementary Fig. 5). Furthermore, the increase in glu/GABA  
184 ratio was not observed during periods immediately before or after recall (Fig. 3a-b;  
185 Supplementary Fig. 6). These findings cannot be explained by differences in data quality  
186 measures between the 'remembered' and 'forgotten' conditions (Supplementary Fig. 7).  
187 Moreover, no effect was observed in NAA, which has overlapping peaks with GABA but is

188 found at higher concentration (Supplementary Fig. 8). Thus, we propose this transient increase  
189 in neocortical glu/GABA ratio reflects a mechanism for associative memory recall.

190

191 As an additional control, we assessed changes in glu/GABA ratio during a subset of  
192 conditioning trials (Supplementary Fig. 9a) that were interleaved with the inference test trials  
193 during the MRI scan and shared the same temporal structure. Importantly, previous studies  
194 suggest performance on conditioning trials is not hippocampal-dependent<sup>33</sup>. During the  
195 conditioning trials, we observed no change in glu/GABA ratio during presentation of the visual  
196 cue or outcome, relative to the ITI period (Supplementary Fig. 9b-c).

197

### 198 **A hippocampal index for fluctuations in neocortical glu/GABA ratio**

199 We next asked which brain regions coordinate this transient break in neocortical glu/GABA  
200 ratio during memory recall. The hippocampus is a promising candidate, given this brain region  
201 supports memory<sup>3</sup> and shows activity modulation during the inference test (Fig. 2c). To test  
202 this possibility, we took advantage of our simultaneous fMRI-fMRS acquisition (Fig. 2a). We  
203 hypothesized that the increase in hippocampal BOLD signal observed during recall (Fig. 2c)  
204 should predict the increase in glu/GABA ratio observed in V1 (Fig. 3). In line with this  
205 prediction, across participants the hippocampal BOLD signal negatively predicted the relative  
206 concentration of GABA and positively predicted the increase in glu/GABA ratio in V1  
207 ('remembered' versus 'forgotten' trials; Fig. 4a-b). Furthermore, across the imaged brain  
208 volume (Fig. 2a), only the hippocampus significantly predicted the increase in V1 glu/GABA  
209 ratio on 'remembered' versus 'forgotten' trials (Fig. 4c). Finally, this relationship between the  
210 hippocampus and glu/GABA ratio was specific to the recall period during the inference test  
211 (Fig. 4d, Supplementary Fig. 10).

212

## 213 **DISCUSSION**

214 The hippocampus is thought to provide an index for memories stored across distributed  
215 neocortical circuits<sup>7-9</sup>. However, the mechanism by which hippocampal activity is coordinated  
216 with neocortex to facilitate memory recall has remained unclear. Here, using time-resolved  
217 fMRI-fMRS in humans, we show that recall of a visual cue is accompanied by a dynamic  
218 increase in the ratio between glutamate and GABA in visual cortex. This transient increase in  
219 glu/GABA ratio in visual cortex is selectively predicted by activity in the hippocampus.  
220 Accordingly, we propose the hippocampus gates recall of memories stored across distributed  
221 neocortical circuits using a disinhibitory mechanism (Fig. 4e). This mechanism may explain



222 how a memory index represented by the hippocampus selectively releases otherwise dormant  
223 representations stored across distributed neocortical circuits.

224

225 Memory recall via a disinhibitory mechanism may be supported by neural circuits identified in  
226 rodents, where glutamatergic projections from higher-order or interconnected brain regions  
227 have the capacity to instantiate highly specific disinhibition in cortical circuits<sup>13,44,45</sup>. For  
228 example, to enhance visual discrimination during attentional modulation, projections from the  
229 cingulate region of mouse frontal cortex modulate activity in V1 by targeting vasoactive  
230 intestinal polypeptide-expressing (VIP+) interneurons, which in turn preferentially target other  
231 interneuron subtypes to release excitatory principle cells from inhibitory control<sup>13</sup>. During  
232 memory recall, hippocampal projections may similarly instantiate highly specific disinhibitory  
233 control over cortical circuits to permit memory reinstatement. These findings are consistent  
234 with causal manipulations in humans showing that the hippocampus predicts memory  
235 expression in sensory neocortex unless neocortical glu/GABA ratio is disturbed<sup>46</sup>. Our results  
236 explain findings in humans showing that hippocampal GABA and glutamate can predict  
237 mnemonic control<sup>47,48</sup> and may account for coordinated hippocampal-neocortical memory  
238 reinstatement reported in human imaging studies<sup>37</sup> and intracranial recordings in epilepsy  
239 patients<sup>10</sup>. Moreover, hippocampal mediated neocortical disinhibition may potentially provide  
240 a signature for coordinated ripple-burst oscillatory activity between hippocampus and  
241 neocortex that has previously been observed in humans during memory recall<sup>49</sup>.

242

243 Our findings further speak to evidence reported from animal models showing that the ratio of  
244 excitatory to inhibitory synaptic conductance remains invariant, fluctuating around a stable set  
245 point<sup>50</sup>. While this may ensure that neurons and networks are neither hypo- nor hyper-excitable  
246 for prolonged periods, the exact E/I ratio is highly dynamic. Evidence in humans, animal  
247 models and theoretical models together suggest overall proportionality between excitation and  
248 inhibition is maintained to hold memories in a silent and dormant state<sup>30-32,51</sup>, thus protecting  
249 memories from interference caused by new learning<sup>46,52</sup>. Within this framework, memories  
250 must be released from inhibitory control to permit recall. While the precise mechanism may  
251 vary across brain systems and circuits, our data suggest disinhibition in V1 can release  
252 excitatory ensembles from balanced inhibition. Moreover, at the microcircuit level,  
253 disinhibition during memory recall has previously been identified following fear  
254 conditioning<sup>53,54</sup>. Thus, in addition to the established function of local disinhibition in



255 promoting initial encoding of memory<sup>11,45</sup>, disinhibition may play a significant role in  
256 facilitating release and recall of previously learned but latent cortical associations.

257

258 During memory recall, we report a transient break in the glutamate/GABA ratio which can be  
259 attributed to a decrease in the concentration of MRS-derived GABA. The quality of the MRS  
260 data was comparable with other 7T MRS studies using unedited sequences to study glutamate  
261 and GABA in visual cortex<sup>41,42,55,56</sup>, as well as previous studies employing event-related  
262 fMRS<sup>40,43,57</sup>. While it is tempting to equate these changes in neurometabolite concentration  
263 with changes in synaptic activity, rapid changes in synaptic glutamate and GABA that  
264 accompany neurotransmitter release occur on a time-scale that is not possible to detect using  
265 the fMRI-fMRS sequence implemented here. Moreover, only a fraction of MRS-derived  
266 neurometabolite concentration reflects neurotransmitter release. MRS-derived measures fail to  
267 discriminate between different pools of glutamate and GABA (cytoplasmic, vesicular, or  
268 extracellular) and metabolites in different cellular compartments are maintained by a variety  
269 of different homeostatic mechanisms. MRS is considered most sensitive to unconstrained,  
270 intracellular metabolic pools that reside at relatively high concentration in the neuronal  
271 cytoplasm<sup>58</sup>. By comparison, changes in extracellular GABA of less than 100-fold are unlikely  
272 to be detectable using MRS<sup>59</sup> and post-mortem studies suggest MRS is not sensitive to  
273 intracellular pools that reside in the mitochondria or vesicles<sup>60,61</sup>.

274

275 Interpretation of MRS-derived glutamate and GABA is further complicated by the fact that the  
276 release and recycling of glutamate and GABA constitute major metabolic pathways<sup>21,22</sup>. Yet,  
277 the metabolic and neurotransmitter pools are thought to be tightly coupled during anaesthesia,  
278 rest and certain stimulation protocols, with a 1:1 relationship reported between the rate of  
279 glutamine-glutamate cycling, which is necessary for glutamate and GABA synthesis, and  
280 neuronal oxidative glucose consumption, which indirectly supports neurotransmitter release  
281 among other processes<sup>23-25</sup>. Therefore, an increase in synaptic neurotransmission occurs  
282 together with an increase in synthesis of exogenous glutamate, which provides a precursor for  
283 GABA via the glutamate-glutamine cycle. During sensory stimulation a transient uncoupling  
284 has been observed with a short-lived mismatch between glucose utilization and oxygen  
285 consumption<sup>62,63</sup>, particularly during stimulation protocols that alternate between high intensity  
286 and quiescent periods<sup>64</sup>. Dynamic fluctuations in fMRS-derived glutamate and GABA reported  
287 here may therefore reflect transitions to new metabolic steady states<sup>65</sup>, which could reflect (if  
288 indirectly) relative shifts in EI equilibrium at the physiological level. During associative

289 memory recall, the increase in glutamate/GABA ratio may be interpreted as an increase in  
290 synthesis of glutamate relative to degradation, with an opposing effect on GABA.

291

292 This interpretation is supported by a handful of previous studies showing event-related changes  
293 in MRS glutamate<sup>40,43,57</sup> and GABA<sup>66</sup>, together with a growing body of evidence reporting a  
294 relationship between MRS-derived measures of neurometabolites and behaviour<sup>67–</sup>  
295 <sup>69</sup>. Nevertheless, it remains to be established whether unconstrained glutamatergic and  
296 GABAergic pools show event-related changes that are MRS-sensitive. To validate this  
297 interpretation of event-related fMRS it is important to leverage animal studies where more  
298 sensitive methods can be employed to relate fMRS measures to physiological parameters. Here,  
299 by implementing an inference task in VR, we operationalize memory recall using the exact  
300 same paradigm previously employed in rodents<sup>33</sup>. Therefore, in addition to engaging attention  
301 and memory-dependent inference, “opening the box” to find a reward in the VR environment  
302 approximated the process of rodents finding a reward from a dispenser in a 3D environment.  
303 By using VR, the findings presented here may be compared to data acquired in animal models  
304 in ongoing future research. In this manner, VR paradigms in humans may provide a basis from  
305 which to gain insight into the cellular and circuit mechanisms that underlie macroscopic  
306 measures of excitation and inhibition. This may prove particularly useful for establishing a  
307 more detailed understanding of the relationship between fMRS-derived measures of glutamate  
308 and GABA and physiological measures of EI balance.

309

310 Previous fMRS protocols typically employ a ‘block’ design, where a static measure of the  
311 concentration of glutamate and GABA is achieved by averaging the spectra across a time-  
312 window that may span several minutes. The clear limitation of this approach is that dynamic  
313 changes in glutamate and GABA are not assessed in relation to cognitive processes and  
314 ongoing behaviour that occur on a much faster scale. With the increase in availability of ultra-  
315 high field MRI scanners and the development of more advanced sequences<sup>70</sup>, fMRS has  
316 emerged as a viable method to detect dynamic changes in neurochemicals in both healthy and  
317 clinical populations<sup>65</sup>. Although there are currently only a handful of event-related fMRS  
318 studies, together with our data, these suggest fMRS is highly sensitive to detecting task-  
319 relevant dynamic changes in glutamate and GABA<sup>71</sup>. For example, in the lateral occipital  
320 complex fMRS demonstrates differences in glutamate in response to presentation of objects  
321 versus abstract stimuli<sup>57</sup>, and in the left anterior insula fMRS reveals a transient increase in  
322 glutamate with exposure to painful stimuli<sup>40</sup>. fMRS-derived glutamate is even sufficiently

323 sensitive to detect repetition suppression effects in the lateral occipital complex<sup>43</sup>, mirroring  
324 analogous effects reported in fMRI<sup>72</sup>. Here, we further illustrate that within a 3 second window  
325 delineated by the question period in the inference task, the temporal resolution of fMRS is  
326 sufficient to relate transient changes in glutamate and GABA to memory performance. fMRS  
327 therefore provides a promising tool to capture real-time, task-relevant changes in  
328 neurometabolites, on a time scale equivalent to task-based fMRI. Assessing whether the  
329 temporal resolution of fMRS can be further improved will likely prove an important step in  
330 refining fMRS in the future.

331

332 During associative memory recall, the transient increase in glu/GABA ratio reported in our  
333 data can primarily be accounted for by a significant decrease in the concentration of MRS-  
334 derived GABA, which was in turn predicted by the hippocampal BOLD signal. Notably,  
335 detecting dynamic changes in GABA is challenging for two key reasons: the concentration of  
336 GABA in human brain tissue is relatively low and the spectral peaks for GABA overlap with  
337 other, more abundant neurochemicals<sup>73-75</sup>. While the most common approach to detecting  
338 MRS-derived GABA involves using a J-difference spectral editing technique to separate peaks  
339 that derive from GABA from overlapping peaks<sup>76,77</sup>, here we use a non-edited sequence  
340 (sLASER). While spectral editing may provide higher precision<sup>56</sup>, this occurs at the cost of a  
341 larger volume of interest and longer TEs, which makes it less suitable for event-related  
342 fMRS<sup>78,79</sup>. Moreover, direct comparisons between edited and non-edited sequences at 7T  
343 reveal no significant difference in the concentration of GABA measurements<sup>56</sup>. Therefore,  
344 together with studies reporting dynamic changes in GABA with sensory stimulation<sup>55,80</sup>, our  
345 data illustrates how a non-edited sequence can provide sufficient data quality for measuring  
346 dynamic changes in MRS-derived GABA, which cannot be explained by changes in  
347 compounds at higher-concentration that have overlapping peaks (i.e. glutamate or NAA,  
348 Supplementary Fig. 8). Moreover, compared to spectral editing, our approach comes with the  
349 advantage of simultaneously measuring dynamic changes in GABA and glutamate, together  
350 with 17 other neurometabolites.

351

352 Disturbances in EI balance are thought to underlie a number of neuropsychiatric conditions,  
353 including schizophrenia, autism, epilepsy and Tourette's syndrome<sup>65,81,82</sup>. While previous  
354 studies report inconsistencies in MRS-derived measures of glutamate and GABA in these  
355 patient populations, this may be attributed to differences in brain region, cognitive state and  
356 imaging protocol, among other factors. Here, by using both fMRS and fMRI to reveal a

357 signature change in glu/GABA ratio that relates to hippocampal BOLD signal, behavioural  
358 performance and cognition, our findings present a potential target for clinical investigation.

359

360 In summary, using time-resolved fMRI-fMRS we report a transient increase in glu/GABA ratio  
361 in V1 during associative recall of a visual cue. This increase in glu/GABA ratio can be  
362 attributed to a decrease in the concentration of MRS-derived GABA, which is predicted by  
363 activity in the hippocampus. By unveiling this coordination between the hippocampus and  
364 neocortex, we show how the hippocampus may have the capacity to selectively modulate and  
365 disinhibit memories represented in neocortex. This mechanism may explain how the  
366 hippocampus plays a key role in memory recall, by indexing the release of specific memories  
367 stored across distributed neocortical circuits.

368

369

370

371

372

373

374

375

376

377

378

379

380

381

382

383

384

385

386

387

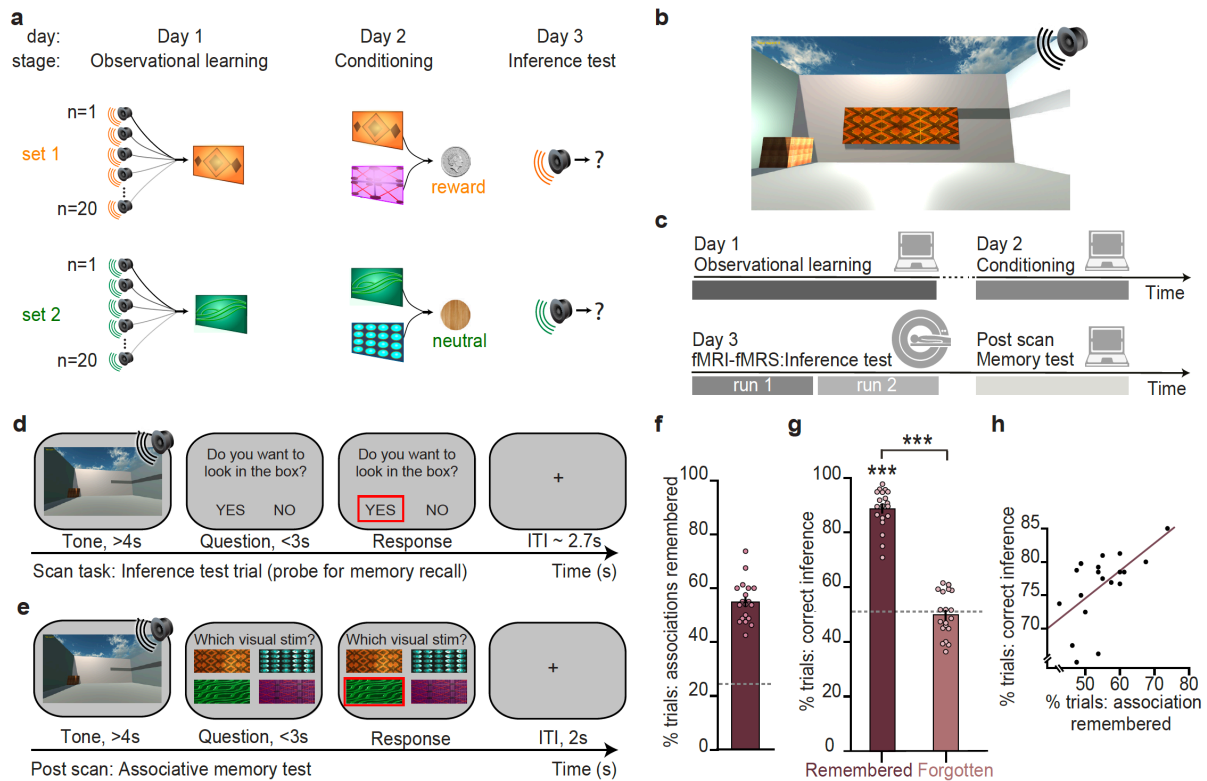
388

389

390

391 MAIN FIGURES

392



393

394

395

396

397

398

399

400

401

402

403

404

405

406

407

408

409

410

411

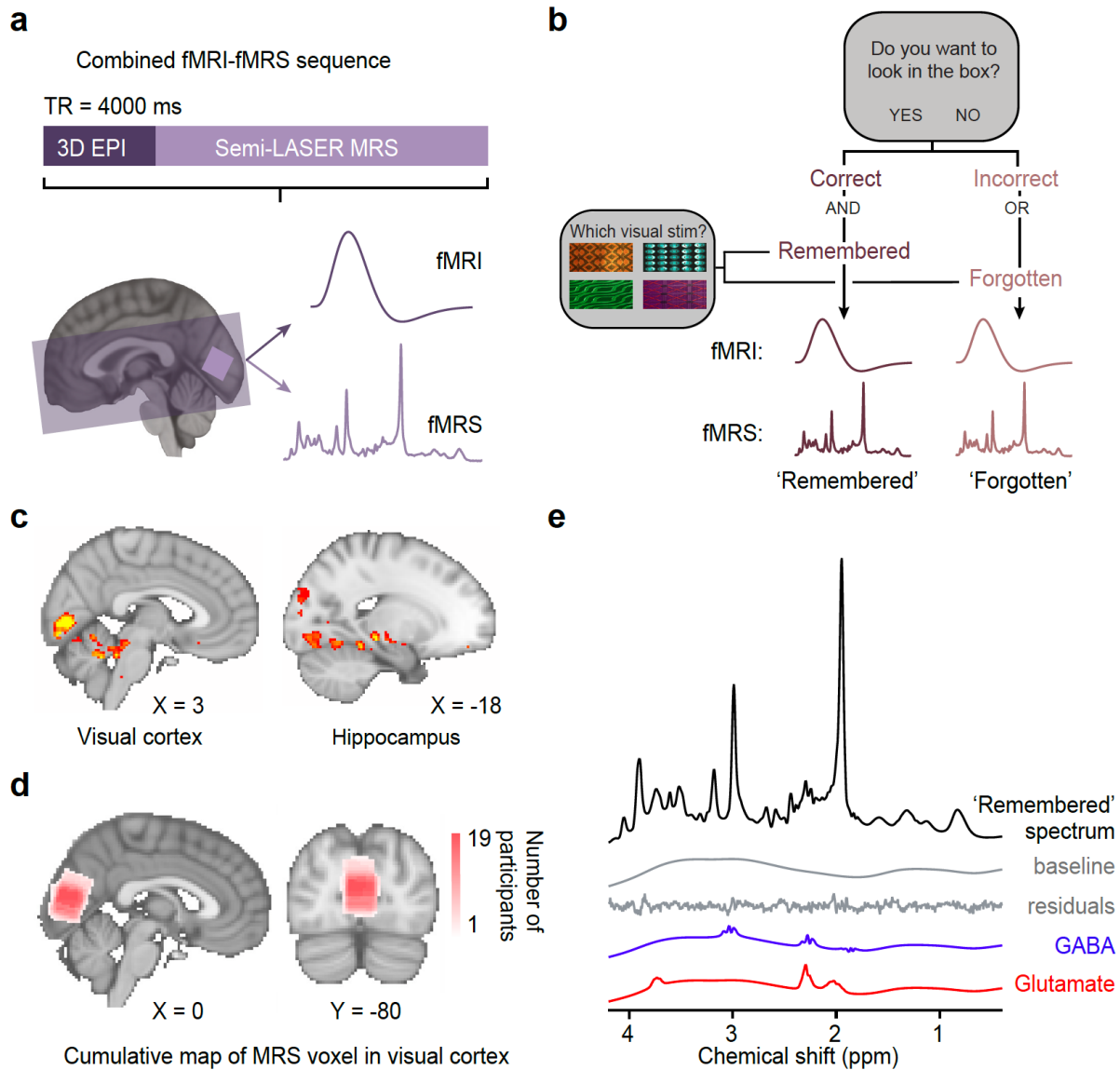
412

413

414

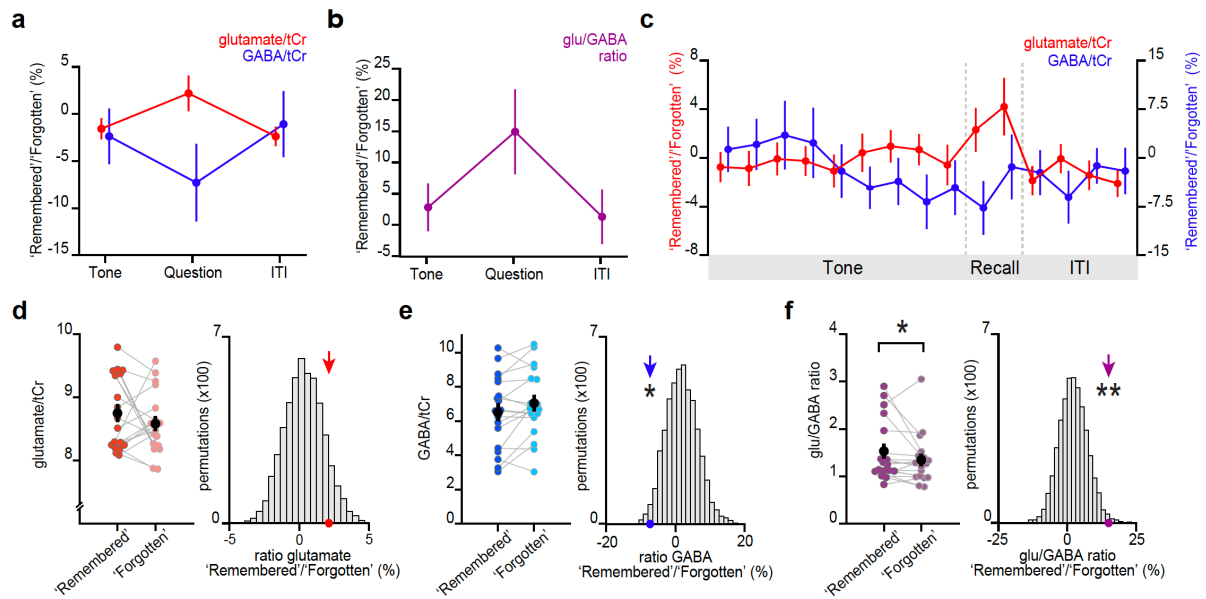
**Figure 1 | Inference task design and behavioural performance.**

**a** Three-stage inference task designed to investigate hippocampal-dependent associative memory recall. First, participants learned to associate auditory cues with visual cues ('observational learning' stage, day 1), where four different visual cues were each associated with 20 auditory cues. Second, participants learned to associate visual cues with an outcome ('conditioning' stage, day 2), where two visual cues predicted a rewarding outcome (set 1, monetary coin) while the other two predicted a neutral outcome (set 2, woodchip). Third, the auditory cues were played in isolation and we assessed participants' ability to infer the relevant outcome ('inference test', day 3). **b** The three-stage inference task shown in **a** was performed within a virtual-reality environment. **c** Schematic: training and testing protocol. The inference test was performed inside the 7T MRI scanner. After completion of the three-stage inference task participants were given a surprise memory test (day 3). **d** Example inference test trial performed inside the scanner. For each auditory cue, participants were required to infer whether they would like to look in the wooden box, where the outcome cues were delivered during conditioning. **e** Example trial from the surprise post-scan associative memory test. **f** During the post-scan associative memory test participants remembered 55% of the auditory-visual associations ( $54.8 \pm 1.78\%$ ; mean  $\pm$  SEM), significantly above chance as indicated by the dotted line ( $t_{18}=16.80$   $p<0.001$ ). **g** Behaviour during the inference test (Fig. 1d) was assessed as correct if participants pressed 'yes' for auditory cues in set 1, or 'no' for auditory cues in set 2. Participants successfully inferred on trials for which the auditory-visual association was later remembered ('later remembered':  $t_{18}=22.91$ ,  $p<0.001$ ; 'later forgotten':  $t_{18}=0.09$ ,  $p=0.925$ ; 'later remembered' – 'later forgotten':  $t_{18}=16.21$ ,  $p<0.001$ ; dotted line indicates chance). **h** Across participants, behavioural performance on the inference test was predicted by behavioural performance on the post-scan associative memory test ( $r_{17}=0.57$ ,  $p=0.010$ ). Notably, there was no significant effect of sex on behavioural performance (Supplementary Table 1).



415  
 416 **Figure 2 | Using fMRI-fMRS data to assess changes in BOLD signal and glu/GABA ratio during the inference test**  
 417 a 7T MRI sequence. 3D BOLD echo planar imaging (3D-EPI) and semi-LASER MR-spectroscopy were acquired in the same  
 418 TR. The MRS voxel was positioned in V1 (light-purple) and the EPI slice coverage included occipital and temporal lobes  
 419 (dark-purple). b Schematic showing how trials during the inference test were categorized into ‘remembered’ and ‘forgotten’.  
 420 Trials were categorised as ‘remembered’ if participants correctly inferred the appropriate outcome during the inference test *and*  
 421 subsequently recalled the auditory-visual association in the post-scan memory test. Trials were categorised as ‘forgotten’ if  
 422 participants incorrectly inferred the appropriate outcome during the inference test *or* subsequently forgot the auditory-visual  
 423 association in the post-scan memory test. c During the question period in the inference test (Fig. 1c-d), BOLD signal in the  
 424 visual cortex and the hippocampus was significantly higher for ‘remembered’ versus ‘forgotten’ auditory cues (‘remembered’  
 425 – ‘forgotten’, visual cortex:  $t_{17}=6.93$ ,  $p<0.001$ ; left hippocampus:  $t_{17}=4.36$ ,  $p=0.017$ ; whole-volume FWE-corrected; together  
 426 with regions listed in Supplementary Table 3). d Anatomical location of 2x2x2 cm<sup>3</sup> MRS voxel positioned in V1. Cumulative  
 427 map across participants. e Representative MRS spectrum from ‘remembered’ trials in the inference test, for an example subject.  
 428 Top to bottom: average spectra, baseline, residuals, estimated GABA, estimated glutamate.  
 429



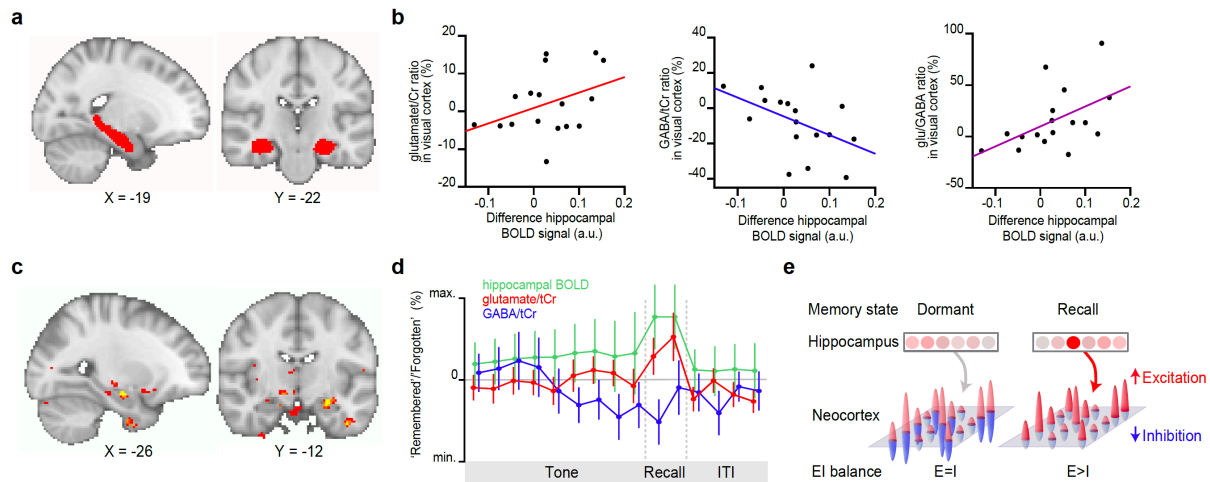


430  
431  
432  
433  
434  
435  
436  
437  
438  
439  
440  
441  
442  
443  
444  
445  
446

**Figure 3 | Memory recall and inference involves a transient break in glu/GABA ratio**

a-b During the question period of the inference test trials (up to 3 s), glu/GABA ratio significantly increased during ‘remembered’ versus ‘forgotten’ trials (‘remembered’:‘forgotten’, glu/GABA ratio:  $t_{17}=2.19$ ,  $p=0.042$ ). This break in glu/GABA ratio was not observed during the ‘tone’ (~7 s) or ‘ITI’ (~2.7 s) periods (‘Tone’, glu/GABA ratio:  $t_{18}=0.74$ ,  $p=0.468$ ; ‘ITI’, glu/GABA ratio:  $t_{18}=0.30$ ,  $p=0.766$ ). Note that glutamate:tCr and GABA:tCr concentrations have been multiplied by 8 as per LCMoDel’s default settings. c Moving average showing glutamate:tCr and GABA:tCr for the ratio of ‘remembered’ to ‘forgotten’ trials during the inference test. Each point represents a 2.5s time bin (mean  $\pm$  SEM). d-f Left: The metabolite values and glu/GABA ratio during the question period for ‘remembered’ and ‘forgotten’ trials (mean  $\pm$  SEM). Right: Comparing the mean ratio of ‘remembered’ to ‘forgotten’ (coloured arrows) against null distributions generated by permuting the trial labels to control for any potential biases in the analyses. Relative to the null distributions, GABA significantly decreased while glu/GABA ratio significantly increased (glutamate:tCr:  $p=0.097$ ; GABA:tCr:  $p=0.015$ ; glu/GABA ratio:  $p=0.009$ ) \* indicates  $p<0.05$ , \*\* indicates  $p<0.01$ .





447  
448  
449  
450  
451  
452  
453  
454  
455  
456  
457  
458  
459

**Figure 4 | Hippocampal BOLD predicts neocortical glu/GABA ratio during recall**

**a** Region of interest (ROI) in the hippocampus (red). **b** Across participants, the increase in hippocampal BOLD signal during ‘remembered’ compared to ‘forgotten’ trials positively predicted the decrease in GABA and the increase in glu/GABA ratio observed in V1 (Fig. 3b-d) (glutamate:tCr:  $r_{16}=0.15$ ,  $p=0.572$ ; GABA:tCr:  $r_{16}=-0.56$ ,  $p=0.022$ ; glu/GABA ratio:  $r_{16}=0.52$ ,  $p=0.033$ ). **c** Across the imaged brain volume, for ‘remembered’ versus ‘forgotten’ trials the correlation between BOLD signal and V1 glu/GABA ratio was selectively observed in the left hippocampus ( $t_{16}=11.25$ ,  $p=0.005$ , whole-brain FWE corrected; Supplementary Table 6). **d** Moving average showing the ratio of ‘remembered’ to ‘forgotten’ trials during the inference test: hippocampal BOLD signal (green,  $n=19$ , range [-4:4]), glutamate:tCr (red,  $n=19$ , range [-8:8]), GABA:tCr (blue,  $n=19$ , range [-15:15]). Each point represents a 2.5s time bin (mean  $\pm$  SEM). **e** Schematic illustrating how the hippocampus may facilitate memory recall of a sensory cue during a transient break in neocortical EI balance.

## 460 **METHODS**

461

### 462 **Participants**

463 22 healthy human volunteers were included in the study (mean age of  $22.8 \pm 0.74$  years, 4 males). All experiments  
464 were approved by the University of Oxford ethics committee (reference number R43594/RE001). All participants  
465 gave informed written consent. For one participant, we were unable to collect combined fMRI-fMRS data due to  
466 time constraints during scanning. Two participants were excluded from the fMRI and fMRS analyses due to  
467 technical difficulties which resulted in the auditory cues not being fully audible during the inference test. Notably,  
468 there was no significant effect of sex on either behavioural performance or MRS measures of glu/GABA ratio  
469 during the inference test (Supplementary Table 1).

470

### 471 **Virtual reality environment**

472 The virtual reality (VR) environment was coded using Unity 5.5.4f1 software (Unity Technologies, CA United  
473 States). The environment was designed to simulate an open field environment previously used to investigate  
474 memory and inference in mice<sup>33</sup>. By incorporating VR, our experimental design is therefore suitable for making  
475 cross-species comparisons in the future. This may prove important when seeking to establish a more refined  
476 interpretation of fMRS in relation to neural circuit mechanisms.

477

478 The environment included a square-walled room with no roof (Fig. 1b). To help evoke the experience of 3D space  
479 and aid orientation within the VR environment, each wall of the environment was distinguished by colour (dark  
480 green, light green, dark grey or light grey), illumination (two walls were illuminated while the other two were  
481 in shadow) and by the presence of permanent visual cues. The permanent visual cues included clouds in the sky, a  
482 vertical black stripe in the middle of the light green wall, a horizontal black strip across the light grey wall, and a  
483 wooden box situated in one corner of the environment. A first-person perspective was implemented and  
484 participants could control their movement through the virtual space using the keyboard arrows (2D translational  
485 motion) and the mouse-pad (head tilt). Movement through the environment elicited the sound of footsteps. Within  
486 the VR environment participants were exposed to a range of different sensory stimuli, in accordance with the  
487 three-stage inference task described below.

488

### 489 **Three-stage inference task**

490 In the VR environment (Fig. 1b) humans performed an inference task (Fig. 1a). The rationale for using an  
491 inference task to assess mechanisms responsible for associative memory was three-fold. First, evidence in both  
492 humans and mice shows that performance on this inference task requires associative memory recall<sup>33</sup>. Second, in  
493 mice, inference, but not first-order associative recall, is hippocampal dependent<sup>33-35</sup>, thus providing an opportunity  
494 to investigate hippocampal dependent associative memory recall. Third, the task can be deployed across humans  
495 and rodents, which may allow future investigation of the cellular mechanisms that underlie non-invasive measures  
496 reported here.

497

498 The task was adapted from associative inference and sensory preconditioning tasks described elsewhere<sup>33,83,84</sup> and  
499 involved 3 stages performed across 3 consecutive days, respectively (Fig. 1a,c). The first and second stages were  
500 performed outside the scanner while the third stage was performed inside the scanner (Fig. 1c). At the start of the  
501 experiment the pairings between auditory, visual and outcome cues were randomly assigned for each participant.

502

503 On day 1, participants performed the ‘observational learning’ stage (Fig. 1a), during which participants were  
504 required to learn at least 40 (out of 80 total) auditory-visual associations via mere exposure. In total, there were 4  
505 visual cues, each associated with 20 different auditory cues. Auditory cues constituted 80 different complex  
506 sounds (e.g. natural sounds or those produced by musical instruments) that were played over headphones. Visual  
507 cues constituted 4 different unique patterned panels which could appear on the walls of the environment (Fig  
508 1a,b,e). To control for potential spatial confounds, two of the visual cues were always presented on the same wall,  
509 the assignment of which was randomized for each participant. The two remaining visual cues were ‘nomadic’,  
510 meaning that with each presentation they were randomly assigned to one of the four walls.

511

512 Training during the observational learning stage occurred within the VR environment and was divided into 8 sub-  
513 sessions. In each sub-session, participants controlled their movement within the VR environment and were  
514 presented with 20 trials in which 10 different auditory-visual associations, different in each sub-session, were  
515 each presented twice, in a random order. On each trial an auditory and visual cue were presented serially and  
516 contiguously: 8 s auditory cue followed by 8 s of the associated visual cue, followed by an ITI of 5 s  
517 (Supplementary Fig. 1a). Participants were given the choice to repeat the sub-session if they so wished. After the  
518 sub-session, learning of auditory-visual associations was monitored outside the VR environment, using an  
519 observational learning test coded in Matlab 2016b using Psychtoolbox (version 3.0.13). On each trial of the

520 observational learning test, 1 auditory cue from the sub-session was presented, followed by presentation of 4  
521 different visual cues (Supplementary Fig. 1b). Participants were instructed to select the visual cue associated with  
522 the auditory cue using a button press response within 3 s, and only at the end of the test were participants given  
523 feedback on their average performance. Each auditory cue in the sub-session was presented 2 times. Participants  
524 were required to repeat training in the VR environment (including the observational learning test) until they  
525 obtained at least 50% accuracy for auditory-visual associations in the sub-session (chance level: 25%).  
526

527 After obtaining at least 50% accuracy on the observational learning test for each sub-session, participants were  
528 given an ‘overview’ memory test (Supplementary Fig. 1b). The memory test had the same format as the  
529 observational learning test used for each sub-session, except that it included all 80 auditory cues, each of which  
530 was presented 3 times. Training on the observational learning stage was terminated when participants reached  
531 >50% accuracy on this ‘overview’ memory test (Supplementary Fig. 1e). If participants failed to reach >50%  
532 accuracy, training in the VR environment was repeated for those sub-sessions with poor performance. Those  
533 participants that failed to reach >50% accuracy on the ‘overview’ memory test (n=3) did not proceed to day 2 and  
534 were thus not included in the experiment.  
535

536 On day 2, participants performed the ‘conditioning’ stage (Fig. 1a), during which they learned that two of the four  
537 visual cues (set 1) predicted delivery of a rewarding outcome (virtual silver coin, as above) on 80% of trials, while  
538 the other two visual cues (set 2) predicted delivery of a neutral outcome (virtual wood-chip, as above) on 100%  
539 of trials. The outcomes were delivered to a wooden box situated in the corner of the environment. To harvest the  
540 value of a virtual silver coin (monetary reward later converted to 20 pence per coin) or a virtual woodchip (no  
541 value, 0 pence), participants were required to first collide with the wooden box, which caused its walls to  
542 disappear, before colliding with the coin or wood-chip which was accompanied by a ‘collision’ sound. The  
543 outcome cues were only available for 10 s. The cumulative total value of harvested reward was displayed in the  
544 upper left corner of the computer screen.  
545

546 Training during the conditioning stage occurred within the VR environment and on each trial, participants were  
547 presented with a visual cue and outcome which were presented serially and contiguously: visual cue (8 s) followed  
548 by outcome delivery to a wooden box (available for 6 s) (Supplementary Fig. 1c). Participants were instructed to  
549 only look in the wooden box after the visual cue was presented and instructed to leave the wooden box before the  
550 next trial. The inter-trial interval (ITI) was 2 s.  
551

552 Learning during the VR conditioning training was monitored using a conditioning test coded in Matlab 2016b  
553 using Psychtoolbox (version 3.0.13). On each trial of the conditioning test, participants were presented with a still  
554 image of a visual cue before being asked to indicate the probability of reward using a number line (Supplementary  
555 Fig. 1d). Participants were given 3 s to respond and were only given feedback on their average performance at the  
556 end of the test. Participants were required to repeat the VR conditioning training and conditioning test until they  
557 performed the test with 100% accuracy (Supplementary Fig. 1f).  
558

559 Finally, on day 3, participants first repeated the conditioning test. Participants then entered the 7T MRI scanner  
560 and performed the ‘inference test’ (Fig. 1a, c-d), together with a subset of conditioning trials (Supplementary Fig.  
561 9a) (see *fMRI-fMRS scan task* below). Immediately after exiting the scanner, participants were given a surprise  
562 associative memory test to assess which auditory-visual associations they remembered and which they had  
563 forgotten (Fig. 1e). The memory test was equivalent to the test performed on day 1 during the observational  
564 learning (Supplementary Fig. 1b), with 3 trials for each auditory stimulus. Performance on auditory-visual  
565 associations was categorised as correct if participants scored 3/3 for that auditory cue on the subsequent surprise  
566 memory test. Performance on auditory-visual associations was categorised as incorrect if participants scored 0/3  
567 or 1/3 for that auditory cue on the subsequent surprise memory test (i.e. no different from chance). Trials where  
568 participants scored 2/3 were not categorised as either correct or incorrect due to their ambiguity. The behavioural  
569 performance measured on the post-scan associative memory test (Fig. 1f) was a more sensitive measure of  
570 memory accuracy than behavioural performance measured during the inference test, with a lower chance level  
571 (associative memory test: 4 choice options with 25% chance level; inference test: 2 options with 50% chance  
572 level) and more repeats of each auditory cue (associative memory test: 3 repeats; inference test: 1 repeat). For this  
573 reason, performance on the inference test during the scan was assessed post-hoc using performance from both the  
574 inference test and the post-scan associative memory test (see *Trial categorisation during the inference test*, Fig.  
575 2b).  
576

#### 577 **fMRI-fMRS scan task**

578 The inference test was incorporated into the fMRI-fMRS scan task. This provided an opportunity to measure  
579 neural responses to associative memory recall required for inferential judgements. The scan task included two

580 different trial types: inference test trials (Fig. 1d) and conditioning trials (Supplementary Fig. 9a). For both types  
581 of trial participants viewed a short video taken from the VR training environment. The videos were presented via  
582 a computer monitor and projected onto a screen inside the scanner bore. On each trial the duration of the video  
583 was determined using a truncated gamma distribution with mean of 7 s, minimum of 4 s and maximum of 14 s.  
584 During the inference test trials, the video of the VR environment was accompanied by an auditory cue, played  
585 over MR compatible headphones (S14 inset earphones, Sensimetrics). Visual cues were not displayed during these  
586 trials: the auditory cues were presented in isolation. At the end of the video, participants were presented with a  
587 question asking: ‘Would you like to look in the box?’, with the options ‘yes’ or ‘no’ (Fig. 1d). Participants were  
588 required to make a response within 3 s using an MR compatible button box and their right index or middle fingers.  
589 No feedback was given. To infer the appropriate outcome participants were instructed to use the learned structure  
590 of the task. The inference test thus provided an opportunity to investigate memory recall: to infer the correct  
591 choice participants needed to recall the appropriate visual cue associated with the auditory cue (Fig. 1g).  
592 Conditioning trials were interleaved with inference test trials to minimise extinction effects. During conditioning  
593 trials, the video of the VR environment orientated towards a visual stimulus displayed on one of the four walls  
594 (Supplementary Fig. 9a). At the end of the video, participants were presented with a still image of the associated  
595 outcome for that visual cue (Supplementary Fig. 9a). After each trial (inference or conditioning) a cross was  
596 presented in the centre of the screen during an inter-trial interval of varying length, determined using a truncated  
597 gamma distribution (mean of 2.7 s, minimum of 1.4 s, maximum of 10 s).

598  
599 To control for potential confounding effects of space, each video during the inference test involved a trajectory  
600 constrained to a 1/16 quadrant of the VR environment, evenly distributed across the different auditory cues. Across  
601 conditioning trials, each visual cue was presented 16 times, once in each possible spatial quadrant. The fMRI-  
602 fMRS scan task was evenly divided across 2 scan blocks, each of which lasted 15 minutes. The fMRI-fMRS scan  
603 task was then repeated (2 more scan blocks) using a higher quality multiband fMRI sequence (not reported here).

#### 604 **fMRI-fMRS data acquisition**

605  
606 The fMRI-fMRS scan task was performed inside a 7 Tesla Magnetom MRI scanner (Siemens) using a 1-channel  
607 transmit and a 32-channel receive phased-array head coil (Nova Medical Inc., USA) at the Wellcome Centre for  
608 Integrative Neuroimaging Centre (University of Oxford). Current 7T radio-frequency (RF) coil designs suffer  
609 from  $B_1^+$  inhomogeneity. To overcome this, we positioned two  $110 \times 110 \times 5 \text{ mm}^3$  Barium Titanate dielectric  
610 pads (4:1 ratio of  $\text{BaTiO}_3:\text{D}_2\text{O}$ , relative permittivity around 300) over occipital lobe, causing a “hotspot” in the  
611 proximal  $B_1^+$  distribution at the expense of distal regions<sup>85</sup>. For each participant, a T1-weighted structural image  
612 was acquired to inform placement of the MRS voxel in visual cortex, and to correct for geometric distortions and  
613 perform co-registration between EPIs, consisting of 176 0.7 mm axial slices, in-plane resolution of  $0.7 \times 0.7 \text{ mm}^2$ ,  
614  $\text{TR} = 2.2 \text{ s}$ ,  $\text{TE} = 2.96 \text{ ms}$ , and field of view = 224 mm. For each participant, a field map with dual echo-time  
615 images was also acquired ( $\text{TE}_1 = 4.08 \text{ ms}$ ,  $\text{TE}_2 = 5.1 \text{ ms}$ , whole-brain coverage, voxel size  $2 \times 2 \times 2 \text{ mm}^3$ ).

616  
617 Fig. 2a shows a diagram of the combined fMRI-fMRS sequence, based on a sequence developed by Hess et al.<sup>86</sup>,  
618 and previously used to compare the BOLD signal in V1 with measures of glutamate<sup>36</sup>. In the same TR of 4s,  
619 BOLD-fMRI (3D EPI, resolution  $2.3 \times 2.3 \times 2.2 \text{ mm}^3$ ; flip angle=5°, repetition time  $\text{TR}_{\text{epi}} = 59 \text{ ms}$ ,  $\text{TE} = 29 \text{ ms}$ ,  
620 field of view 200 mm, 32 slices) and fMRS data ( $2 \times 2 \times 2 \text{ cm}^3$  voxel positioned in the occipital lobe, centered  
621 along the midline and the calcarine sulcus) were acquired. fMRS data were acquired using short-echo-time semi-  
622 localisation by adiabatic selective refocusing (semi-LASER) pulse sequence ( $\text{TE} = 36 \text{ ms}$ ,  $\text{TR}_{\text{mrs}} = 4 \text{ s}$ ) with VAPOR  
623 water suppression and outer volume suppression<sup>87</sup>. A delay between fMRI and fMRS acquisition (250 ms) was  
624 inserted to minimize potential eddy current effects from the EPI read-out<sup>86</sup>. Compared to an uncombined  
625 contemporary MR sequences (e.g. multiband EPI and semi-LASER MRS), the fMRS was of comparable quality,  
626 while the quality of the fMRI component was compromised. On average, 457 fMRS spectra were acquired over  
627 the two scanning blocks (SD: 35.62).

628  
629 In addition to the fMRI-fMRS sequence acquisition, an additional set of fMRI data (reported elsewhere<sup>33</sup> and not  
630 shown here) was acquired using a multiband EPI sequence (50 1.5 mm thick transverse slices with 1.5 mm gap,  
631 in-plane resolution of  $1.5 \times 1.5 \text{ mm}^2$ ,  $\text{TR} = 1.512 \text{ s}$ ,  $\text{TE} = 20 \text{ ms}$ , flip angle = 85°, field of view 192 mm, and multi-  
632 band acceleration factor of 2). To increase SNR in brain regions for which we had prior hypotheses, both the  
633 fMRI sequences were restricted to partial brain coverage (Fig. 2a, covering the occipital and temporal lobes) to  
634 shorten the EPI TR, thus acquiring more measurements.

#### 635 **Trial categorisation during the inference test**

636  
637 Trials during the inference test were categorised into two conditions, ‘remembered’ and ‘forgotten’ (Fig. 2b). To  
638 obtain the most accurate estimate of associative memory recall during the inference test our definition for  
639 ‘remembered’ and ‘forgotten’ derived from behavioural performance on both the inference test and the post-scan



640 associative memory test. Trials where participants made both the correct inference during the inference test *and*  
641 subsequently remembered the auditory-visual association during the post-scan associative memory test were  
642 classified as ‘remembered’. Trials where participants made *either* the incorrect inference during the inference test  
643 *or* subsequently forgot the auditory-visual associations during the post-scan associative memory test were  
644 classified as ‘forgotten’.

#### 646 **fMRS metabolite quantification and analysis**

647 For each scan run, fMRS data from 19 subjects was preprocessed separately in MRspa, a semi-automated  
648 MATLAB routine (<https://www.cmrr.umn.edu/downloads/mrspa/>). The unsuppressed water signal acquired from  
649 the same VOI was used to remove residual eddy current effects and combine individual coil spectra. Spectra were  
650 corrected for frequency and phase variations induced by participants’ motion, and the residual water component  
651 was removed using Hankel Lanczos Singular Value Decomposition (HLSVD). For each participant, spectra from  
652 all blocks were frequency aligned to account for frequency differences between blocks.

653  
654 Spectra were then analysed in an event-related manner. For each participant, the preprocessed spectra were first  
655 assigned to the tone/question/ITI periods by aligning the time stamps for the spectra to the time stamps for each  
656 event recorded during the inference task. Then, spectra acquired within the tone/question/ITI periods were  
657 selected for analysis. Next, these selected spectra were separated into two categories according to task  
658 performance, ‘remembered’ or ‘forgotten’ (Fig. 2b, see *Trial categorisation during the inference test*), before  
659 being analysed using LCModel. Participants (n=1) with less than 8 spectra for either the ‘remembered’ or  
660 ‘forgotten’ conditions were excluded from the fMRS analysis, as previous studies report minimal change in test-  
661 retest CoVs when going from 8 to 16 spectra<sup>88</sup>. Metabolite concentrations for the average ‘remembered’ and the  
662 average ‘forgotten’ spectrum were quantified in turn using LCModel<sup>89</sup> within the chemical shift range 0.5 to 4.2  
663 ppm. The concentration of each metabolite was assessed relative to the concentration of total Creatine (Creatine  
664 + phosphocreatine, tCr), thus providing effective control for variation in voxel tissue and cerebral spinal fluid  
665 (CSF) in the fMRS voxel used across participants. A basis set containing stimulated model spectra of alanine  
666 (Ala), aspartate (Asp), ascorbate/vitamin C (Asc), glycerophosphocholine (GPC), phosphocholine (PCho),  
667 creatine (Cr), phosphocreatine (PCr), GABA, glucose (Glc), glutamine (Gln), glutamate (Glu), glutathione (GSH),  
668 myo-inositol (myo-Ins), Lactate, N-acetylaspartate (NAA), N-acetylaspartylglutamate (NAAG),  
669 phosphoethanolamine (PE), scyllo-inositol (scyllo-Ins), taurine (Tau) and experimentally measured  
670 macromolecules was used. To evaluate the dynamic range of metabolites between ‘remembered’ and ‘forgotten’  
671 conditions, it was not appropriate to use the default settings in LCModel that normalise metabolite estimates such  
672 as GABA to constrain the dynamic range. We therefore removed these prior constraints within LCModel by  
673 setting the ‘*nratio*’ parameter to 0. Estimates normalised to tCr were multiplied by 8, as per convention.

674  
675 Changes in the relative concentration of glutamate and GABA between ‘remembered’ and ‘forgotten’ conditions  
676 were evaluated together with ‘glu/GABA ratio’ which we defined as the ratio of glutamate to GABA<sup>39</sup>. We defined  
677 the change in glutamate, GABA and glu/GABA for ‘remembered’ vs ‘forgotten’ trials as a ratio, as follows:  
678

$$679 \quad \text{Glutamate ratio} = 100 \times \left( \frac{Glu_{remem} - Glu_{forgot}}{Glu_{forgot}} \right)$$

$$680 \quad \text{GABA ratio} = 100 \times \left( \frac{GABA_{remem} - GABA_{forgot}}{GABA_{forgot}} \right)$$

$$681 \quad \text{glu/GABA ratio} = 100 \times \left( \frac{Glu_{remem}/GABA_{remem} - Glu_{forgot}/GABA_{forgot}}{Glu_{forgot}/GABA_{forgot}} \right)$$

682  
683  
684  
685 Where Glu and GABA represent the ratio of glutamate and GABA to total Creatine, respectively, during the  
686 tone/question/ITI period of ‘remembered’ or ‘forgotten’ trials. This ratio effectively controls for variation in voxel  
687 tissue and CSF fraction in the MRS voxel used across participants.

688  
689  
690 Further, to control for differences in the number of ‘remembered’ and ‘forgotten’ spectra, we compared the group  
691 mean difference between ‘remembered’ and ‘forgotten’ trials against a null distribution generated by permuting  
692 the trial labels while preserving differences in number of trials for each participant. On each of 5000 permutations,  
693 the condition labels (‘remembered’, ‘forgotten’) were shuffled for each participant using MATLAB’s random

694 number generator. The relative metabolite concentrations for each condition were then estimated in LCModel and  
695 the difference between conditions computed. The group mean for each permutation was then added to the null  
696 distribution. The difference between ‘remembered’ and ‘forgotten’ conditions derived from the unshuffled data  
697 was then compared against the null distribution generated from the shuffled data (Fig. 3d-f; Supplementary Fig.  
698 5-8).

699

### 700 **fMRI preprocessing and GLMs**

701 Preprocessing of MRI data was carried out using SPM12 (<http://www.fil.ion.ucl.ac.uk/spm/>). First, the anterior  
702 commissure was set to the origin in the anatomical images and in the first volume of each fMRI block, with  
703 equivalent transformations applied to all other images within the same block. Second, to account for magnetic  
704 field inhomogeneities, images were corrected for signal bias, realigned to the first volume, corrected for distortion  
705 using field maps, normalised to a standard EPI template. To remove low frequency noise from the pre-processed  
706 data, a high-pass filter was applied to the data using SPM12’s default settings. For each participant and for each  
707 scanning block, the resulting fMRI data was analysed in an event-related manner using a general linear model  
708 (GLM). The GLM was applied to data from both scan task blocks. In addition to the explanatory variables (EVs)  
709 of interest (described below), 6 additional scan-to-scan motion parameters produced during realignment were  
710 included in the GLM as nuisance regressors to account for motion-related artefacts in each task block. The output  
711 of the first-level analysis was then smoothed using a 5-mm full-width at half maximum Gaussian kernel before  
712 being entered into a second level analysis. The sensitivity of our analysis pipeline to detecting stimulus evoked  
713 BOLD activity patterns benefitted from applying the first-level GLM to unsmoothed data and only including  
714 smoothing prior to the second level analysis (Supplementary Fig. 2). One participant was excluded from the fMRI  
715 analyses as the quality of fMRI data in the fMRI-fMRS sequence was too poor to ensure reliable pre-processing.

716

717 For the first-level analyses, three different GLMs were used. Each GLM included 15 EVs per block. In the first  
718 GLM, the first 8 EVs accounted for the question period in the inference test, divided according to performance of  
719 the subject (‘remembered’ or ‘forgotten’, see *Trial categorisation during the inference test*), before being further  
720 divided according to the 4 possible visual cues to which the auditory cues were associated. The next 4 EVs  
721 accounted for presentation of the visual cue during the video of all conditioning trials, divided according to the 4  
722 different visual cues. The final 3 EVs accounted for presentation of the auditory cue during the video in all  
723 inference test trials, the question period in all remaining inference test trials (i.e. trials not categorized as  
724 ‘remembered’ or ‘forgotten’), and the presentation of the outcome in all conditioning trials. To decorrelate the  
725 EVs modelling the auditory and visual cues from those EVs modelling the question and outcome, respectively,  
726 the duration of events within EVs modelling the auditory and visual cues was set using a box-car function to 4 s,  
727 i.e. the minimum duration of the video. The duration of events within EVs modelling the question/outcome were  
728 set to the duration of the question/outcome. All EVs were then convolved with the hemodynamic response  
729 function.

730

731 In the second and third GLMs, the same EVs were included, however the first 8 EVs accounted for the auditory  
732 cue period in the inference test (second GLM), or the inter-trial interval in the inference test (third GLM). In both  
733 cases, the EVs were divided according to performance of the subject (‘remembered’ or ‘forgotten’), as in the first  
734 GLM.

735

### 736 **Univariate fMRI analysis and statistics**

737 Using the output of the GLMs we assessed the difference in the univariate BOLD response between ‘remembered’  
738 and ‘forgotten’ trials during the inference test (as defined in Fig. 2b, *Trial categorisation during the inference*  
739 *test*). The contrast of interest therefore involved contrasting EVs [1:4] (‘remembered’) with EVs [5:8]  
740 (‘forgotten’), using the first GLM (see above). The resulting contrast images (‘remembered’-‘forgotten’) for all  
741 participants were entered into a second-level random effects ‘group’ analysis. We set the cluster-defining  
742 threshold to  $p < 0.01$  uncorrected before using whole-brain family wise error (FWE) to correct for multiple  
743 comparisons, with the significance level defined as  $p < 0.05$  (Fig. 2c, Supplementary Table 3).

744

### 745 **Assessing the relationship between fMRI and fMRS**

746 To assess the relationship between event-related hippocampal BOLD signal and event-related fMRS measures  
747 from V1, we used an anatomical ROI for the hippocampus (Fig. 4a). Capitalising on variance across participants,  
748 the relationship between the BOLD signal for ‘remembered’-‘forgotten’ within this ROI was compared with  
749 equivalent changes in glutamate, GABA and glu/GABA ratio using a Spearman rank correlation. To assess the  
750 selectivity of these effects to the recall period (question) during the inference test, control analyses were performed  
751 using the output of the second and third GLMs, together with equivalent measures of glutamate, GABA and  
752 glu/GABA ratio (Supplementary Fig. 10).

753

754 Next, to assess the relationship between fMRS and the BOLD signal across the entire imaged brain volume, we  
755 repeated the second-level random effects ‘group’ analysis using the output of the first GLM, but now included  
756 group-level covariates for the change in glutamate and GABA for ‘remembered’-‘forgotten’ (i.e. Fig. 3a), along  
757 with 2 ‘nuisance’ regressors that accounted for unwanted variance attributed to differences in age and sex. To  
758 identify brain regions where the BOLD signal for ‘remembered’:‘forgotten’ predicted changes in glu/GABA ratio,  
759 we contrasted the explanatory variables on the covariates for glutamate and GABA (glutamate – GABA) to  
760 generate a single contrast to test statistical significance. We set the cluster-defining threshold to  $p < 0.01$   
761 uncorrected before using whole-brain family wise error (FWE) to correct for multiple comparisons, with the  
762 significance level defined as  $p < 0.05$  (Fig. 4c, Supplementary Table 6).  
763

764 To visualize the time course of fMRI and fMRS across the inference test trials, we estimated a moving average  
765 for both datasets, where each time bin constituted a 2.5 s time window shifted by 0.5 s in each iteration (Fig. 3c,  
766 Fig. 4d, Supplementary Fig. 10c-d). To account for the jitter in the length of the video and in the ITI, trials that  
767 stopped short were excluded from analyses for that time bin. Thus, to ensure each time bin contained a similar  
768 number of spectra, those time bins at the tail end of the jitter (final 3 time bins during the video and the final 2  
769 time bins of the ITI) were enlarged to include broader time windows. For the fMRS, for each participant the  
770 ‘remembered’ and ‘forgotten’ spectrum were calculated for each time bin, and the ratio estimated to give a  
771 measure of ‘remembered’:‘forgotten’ for both glutamate and GABA (Fig. 3c, Fig. 4d, Supplementary Fig. 10c-  
772 d).  
773

774 For the fMRI, for each participant, and for each time bin during the inference test trial, the time course of the  
775 preprocessed BOLD signal was extracted from the hippocampal ROI (Fig. 4a) and from two control ROIs defined  
776 using a 12 mm sphere within our partial epi volume (Fig. 2a). The first control region was positioned at the  
777 junction between parietal and occipital cortex (‘parietal-occipital cortex’) while the second control region was  
778 positioned within the brainstem (Supplementary Fig. 10c-d). For each ROI, the obtained signal for each trial was  
779 resampled using a resolution of 400 ms and regressed against an explanatory variable indicating those trials that  
780 were remembered. To control for differences in baseline BOLD at the start of the trial, we also included a  
781 ‘nuisance’ explanatory variable indicating whether the previous trial was ‘remembered’. We then plotted the  
782 normalized averaged fMRI regression coefficient for ‘remembered’ vs ‘forgotten’ together with the equivalent  
783 glu/GABA ratio time course (Fig. 4d; Supplementary Fig. 10c-d).  
784

#### 785 **DATA AVAILABILITY**

786 Upon publication, data for all figures will be made available made available on GitHub  
787 ([https://github.com/rskool/memory\\_recall](https://github.com/rskool/memory_recall)).  
788

#### 789 **CODE AVAILABILITY**

790 Upon publication, code used to analyse the data for all figures will be made available made available on GitHub  
791 ([https://github.com/rskool/memory\\_recall](https://github.com/rskool/memory_recall)).  
792

793  
794  
795  
796  
797  
798  
799  
800  
801  
802  
803  
804  
805  
806  
807  
808  
809  
810  
811  
812  
813



814 **REFERENCES**

815

816 1. Josselyn, S. A. & Tonegawa, S. Memory engrams: Recalling the past and imagining the  
817 future. *Science* **367**, (2020).

818 2. Buzsáki, G. Neural syntax: cell assemblies, synapsembles and readers. *Neuron* **68**,  
819 362–385 (2010).

820 3. Squire, L. R. Memory and the hippocampus: A synthesis from findings with rats,  
821 monkeys, and humans. *Psychol. Rev.* **99(2)**, 195–231 (1992).

822 4. Felleman, D. J. & Essen, D. C. V. Distributed hierarchical processing in the primate  
823 cerebral cortex. *Cereb. Cortex* **1**, 1–47 (1991).

824 5. Witter, M. P. Organization of the entorhinal—hippocampal system: A review of current  
825 anatomical data. *Hippocampus* **3**, 33–44 (1993).

826 6. Witter, M. P., Groenewegen, H. J., Lopes da Silva, F. H. & Lohman, A. H. Functional  
827 organization of the extrinsic and intrinsic circuitry of the parahippocampal region. *Prog.*  
828 *Neurobiol.* **33**, 161–253 (1989).

829 7. Goode, T. D., Tanaka, K. Z., Sahay, A. & McHugh, T. J. An Integrated Index: Engrams,  
830 Place Cells, and Hippocampal Memory. *Neuron* **107**, 805–820 (2020).

831 8. Teyler, T. J. & DiScenna, P. The role of hippocampus in memory: A hypothesis.  
832 *Neurosci. Biobehav. Rev.* **9**, 377–389 (1985).

833 9. Teyler, T. J. & Rudy, J. W. The hippocampal indexing theory and episodic memory:  
834 updating the index. *Hippocampus* **17**, 1158–1169 (2007).

835 10. Pacheco Estefan, D. *et al.* Coordinated representational reinstatement in the human  
836 hippocampus and lateral temporal cortex during episodic memory retrieval. *Nat.*  
837 *Commun.* **10**, 2255 (2019).

838 11. Letzkus, J. J., Wolff, S. B. E. & Lüthi, A. Disinhibition, a Circuit Mechanism for  
839 Associative Learning and Memory. *Neuron* **88**, 264–276 (2015).

840 12. Barron, H. C., Auksztulewicz, R. & Friston, K. Prediction and memory: A predictive  
841 coding account. *Prog. Neurobiol.* **192**, 101821 (2020).

- 842 13. Zhang, S. *et al.* Long-range and local circuits for top-down modulation of visual cortex  
843 processing. (2014).
- 844 14. Wehr, M. & Zador, A. M. Balanced inhibition underlies tuning and sharpens spike timing  
845 in auditory cortex. *Nature* **426(6965)**, 442–446 (2003).
- 846 15. Okun, M. & Lampl, I. Instantaneous correlation of excitation and inhibition during  
847 ongoing and sensory-evoked activities. *Nat. Neurosci.* **11**, 535–537 (2008).
- 848 16. Haider, B., Duque, A., Hasenstaub, A. R. & McCormick, D. A. Neocortical network  
849 activity in vivo is generated through a dynamic balance of excitation and inhibition. *J.*  
850 *Neurosci.* **26**, 4535–4545 (2006).
- 851 17. Field, R. E. *et al.* Heterosynaptic Plasticity Determines the Set Point for Cortical  
852 Excitatory-Inhibitory Balance. *Neuron* **106**, 842–854 (2020).
- 853 18. McCormick, D. A., Shu, Y.-S. & Hasenstaub, A. Balanced Recurrent Excitation and  
854 Inhibition in Local Cortical Networks. in *Excitatory-Inhibitory Balance: Synapses, Circuits,*  
855 *Systems* (eds. Hensch, T. K. & Fagiolini, M.) 113–124 (Springer US, 2004).  
856 doi:10.1007/978-1-4615-0039-1\_8.
- 857 19. De Graaf, R. A. *In Vivo NMR Spectroscopy: Principles and Techniques.* (John Wiley &  
858 Sons, 2019).
- 859 20. Mangia, S., Giove, F. & DiNuzzo, M. Metabolic Pathways and Activity-Dependent  
860 Modulation of Glutamate Concentration in the Human Brain. *Neurochem. Res.* **37**,  
861 2554–2561 (2012).
- 862 21. Magistretti, P. J. & Allaman, I. A cellular perspective on brain energy metabolism and  
863 functional imaging. *Neuron* **86**, 883–901 (2015).
- 864 22. Bak, L. K., Schousboe, A. & Waagepetersen, H. S. The glutamate/GABA-glutamine  
865 cycle: aspects of transport, neurotransmitter homeostasis and ammonia transfer. *J.*  
866 *Neurochem.* **98**, 641–653 (2006).
- 867 23. Rothman, D. L., Behar, K. L., Hyder, F. & Shulman, R. G. In vivo NMR Studies of the  
868 Glutamate Neurotransmitter Flux and Neuroenergetics: Implications for Brain Function.  
869 *Annu. Rev. Physiol.* **65**, 401–427 (2003).

- 870 24. Shen, J. *et al.* Determination of the rate of the glutamate/glutamine cycle in the human  
871 brain by in vivo <sup>13</sup>C NMR. *Proc. Natl. Acad. Sci.* **96**, 8235–8240 (1999).
- 872 25. Sibson, N. R. *et al.* Stoichiometric coupling of brain glucose metabolism and  
873 glutamatergic neuronal activity. *Proc. Natl. Acad. Sci.* **95**, 316–321 (1998).
- 874 26. Castro-Alamancos, M. A., Donoghue, J. P. & Connors, B. W. Different forms of synaptic  
875 plasticity in somatosensory and motor areas of the neocortex. *J. Neurosci.* **15**, 5324–  
876 5333 (1995).
- 877 27. Trepel, C. & Racine, R. J. GABAergic modulation of neocortical long-term potentiation in  
878 the freely moving rat. *Synapse* **35**, 120–128 (2000).
- 879 28. Floyer-Lea, A., Wylezinska, M., Kincses, T. & Matthews, P. M. Rapid modulation of  
880 GABA concentration in human sensorimotor cortex during motor learning. *J.*  
881 *Neurophysiol.* **95**, 1639–1644 (2006).
- 882 29. Lunghi, C., Berchicci, M., Morrone, M. C. & Russo, F. D. Short-term monocular  
883 deprivation alters early components of visual evoked potentials. *J. Physiol.* **593**, 4361–  
884 4372 (2015).
- 885 30. Barron, H. C. *et al.* Unmasking Latent Inhibitory Connections in Human Cortex to Reveal  
886 Dormant Cortical Memories. *Neuron* **90**, 191–203 (2016).
- 887 31. Vallentin, D., Kosche, G., Lipkind, D. & Long, M. A. Inhibition protects acquired song  
888 segments during vocal learning in zebra finches. *Science* **351**, 267–271 (2016).
- 889 32. Froemke, R. C., Merzenich, M. M. & Schreiner, C. E. A synaptic memory trace for  
890 cortical receptive field plasticity. *Nature* **450**, 425–429 (2007).
- 891 33. Barron, H. C. *et al.* Neuronal Computation Underlying Inferential Reasoning in Humans  
892 and Mice. *Cell* <https://doi.org/10.1016/j.cell.2020.08.035> (2020)  
893 [doi:10.1016/j.cell.2020.08.035](https://doi.org/10.1016/j.cell.2020.08.035).
- 894 34. Bunsey, M. & Eichenbaum, H. Conservation of hippocampal memory function in rats and  
895 humans. *Nature* **379**, 255–257 (1996).
- 896 35. DeVito, L. M., Kanter, B. R. & Eichenbaum, H. The hippocampus contributes to memory  
897 expression during transitive inference in mice. *Hippocampus* **20**, 208–217 (2010).

- 898 36. Ip, I. B. *et al.* Combined fMRI-MRS acquires simultaneous glutamate and BOLD-fMRI  
899 signals in the human brain. *NeuroImage* **155**, 113–119 (2017).
- 900 37. Horner, A. J., Bisby, J. A., Bush, D., Lin, W.-J. & Burgess, N. Evidence for holistic  
901 episodic recollection via hippocampal pattern completion. *Nat. Commun.* **6**, 1–11 (2015).
- 902 38. Wimmer, G. E. & Shohamy, D. Preference by Association: How Memory Mechanisms in  
903 the Hippocampus Bias Decisions. *Science* **338**, 270–273 (2012).
- 904 39. Shibata, K. *et al.* Overlearning hyperstabilizes a skill by rapidly making neurochemical  
905 processing inhibitory-dominant. *Nat. Neurosci.* **20**, 470–475 (2017).
- 906 40. Gussew, A. *et al.* Time-resolved functional 1H MR spectroscopic detection of glutamate  
907 concentration changes in the brain during acute heat pain stimulation. *NeuroImage* **49**,  
908 1895–1902 (2010).
- 909 41. Bednařík, P. *et al.* Neurochemical responses to chromatic and achromatic stimuli in the  
910 human visual cortex. *J. Cereb. Blood Flow Metab.* **38**, 347–359 (2018).
- 911 42. Prinsen, H., Graaf, R. A. de, Mason, G. F., Pelletier, D. & Juchem, C. Reproducibility  
912 measurement of glutathione, GABA, and glutamate: Towards in vivo neurochemical  
913 profiling of multiple sclerosis with MR spectroscopy at 7T. *J. Magn. Reson. Imaging* **45**,  
914 187–198 (2017).
- 915 43. Apšvalka, D., Gadie, A., Clemence, M. & Mullins, P. G. Event-related dynamics of  
916 glutamate and BOLD effects measured using functional magnetic resonance  
917 spectroscopy (fMRS) at 3 T in a repetition suppression paradigm. *NeuroImage* **118**,  
918 292–300 (2015).
- 919 44. Lee, S., Kruglikov, I., Huang, Z. J., Fishell, G. & Rudy, B. A disinhibitory circuit mediates  
920 motor integration in the somatosensory cortex. *Nat. Neurosci.* **16**, 1662–1670 (2013).
- 921 45. Krabbe, S. *et al.* Adaptive disinhibitory gating by VIP interneurons permits associative  
922 learning. *Nat. Neurosci.* **22**, 1834–1843 (2019).
- 923 46. Koolschijn, R. S. *et al.* The Hippocampus and Neocortical Inhibitory Engrams Protect  
924 against Memory Interference. *Neuron* **101**, 528–541 (2019).

- 925 47. Nikolova, S., Stark, S. M. & Stark, C. E. L. 3T hippocampal glutamate-glutamine  
926 complex reflects verbal memory decline in aging. *Neurobiol. Aging* **54**, 103–111 (2017).
- 927 48. Schmitz, T. W., Correia, M. M., Ferreira, C. S., Prescott, A. P. & Anderson, M. C.  
928 Hippocampal GABA enables inhibitory control over unwanted thoughts. *Nat. Commun.*  
929 **8**, (2017).
- 930 49. Vaz, A. P., Wittig, J. H., Inati, S. K. & Zaghloul, K. A. Replay of cortical spiking  
931 sequences during human memory retrieval. *Science* **367**, 1131–1134 (2020).
- 932 50. Isaacson, J. S. & Scanziani, M. How Inhibition Shapes Cortical Activity. *Neuron* **72**, 231–  
933 243 (2011).
- 934 51. Vogels, T. P., Sprekeler, H., Zenke, F., Clopath, C. & Gerstner, W. Inhibitory Plasticity  
935 Balances Excitation and Inhibition in Sensory Pathways and Memory Networks. *Science*  
936 **334**, 1569–1573 (2011).
- 937 52. Kuchibhotla, K. V. *et al.* Parallel processing by cortical inhibition enables context-  
938 dependent behavior. *Nat. Neurosci.* **20**, 62–71 (2017).
- 939 53. Wolff, S. B. E. *et al.* Amygdala interneuron subtypes control fear learning through  
940 disinhibition. *Nature* **509**, 453–458 (2014).
- 941 54. Courtin, J. *et al.* Prefrontal parvalbumin interneurons shape neuronal activity to drive fear  
942 expression. *Nature* **505**, 92–96 (2014).
- 943 55. Mekle, R. *et al.* Detection of metabolite changes in response to a varying visual  
944 stimulation paradigm using short-TE 1H MRS at 7 T. *NMR Biomed.* **30**, e3672 (2017).
- 945 56. Hong, D., Rankouhi, S. R., Thielen, J.-W., Asten, J. J. A. van & Norris, D. G. A  
946 comparison of sLASER and MEGA-sLASER using simultaneous interleaved acquisition  
947 for measuring GABA in the human brain at 7T. *PLOS ONE* **14**, e0223702 (2019).
- 948 57. Lally, N. *et al.* Glutamatergic correlates of gamma-band oscillatory activity during  
949 cognition: A concurrent ER-MRS and EEG study. *NeuroImage* **85**, 823–833 (2014).
- 950 58. Rae, C. A Guide to the Metabolic Pathways and Function of Metabolites Observed in  
951 Human Brain 1H Magnetic Resonance Spectra. *Neurochem. Res.* **39**, 1–36 (2014).

- 952 59. Myers, J. F., Nutt, D. J. & Lingford-Hughes, A. R.  $\gamma$ -aminobutyric acid as a metabolite:  
953 Interpreting magnetic resonance spectroscopy experiments. *J. Psychopharmacol. (Oxf.)*  
954 **30**, 422–427 (2016).
- 955 60. De Graaf, A. A. & Bovée, W. M. M. J. Improved quantification of in vivo  $^1\text{H}$  NMR spectra  
956 by optimization of signal acquisition and processing and by incorporation of prior  
957 knowledge into the spectral fitting. *Magn. Reson. Med.* **15**, 305–319 (1990).
- 958 61. Kauppinen, R. A. & Williams, S. R. Nondestructive Detection of Glutamate by  $^1\text{H}$   
959 Nuclear Magnetic Resonance Spectroscopy in Cortical Brain Slices from the Guinea Pig:  
960 Evidence for Changes in Detectability During Severe Anoxic Insults. *J. Neurochem.* **57**,  
961 1136–1144 (1991).
- 962 62. Fox, P. T., Raichle, M. E., Mintun, M. A. & Dence, C. Nonoxidative glucose consumption  
963 during focal physiologic neural activity. *Science* **241**, 462–464 (1988).
- 964 63. Fox, P. T. & Raichle, M. E. Focal physiological uncoupling of cerebral blood flow and  
965 oxidative metabolism during somatosensory stimulation in human subjects. *Proc. Natl.*  
966 *Acad. Sci.* **83**, 1140–1144 (1986).
- 967 64. Gjedde, A., Marrett, S. & Vafaee, M. Oxidative and Nonoxidative Metabolism of Excited  
968 Neurons and Astrocytes. *J. Cereb. Blood Flow Metab.* **22**, 1–14 (2002).
- 969 65. Stanley, J. A. & Raz, N. Functional Magnetic Resonance Spectroscopy: The “New” MRS  
970 for Cognitive Neuroscience and Psychiatry Research. *Front. Psychiatry* **9**, (2018).
- 971 66. Cleve, M., Gussew, A. & Reichenbach, J. R. In vivo detection of acute pain-induced  
972 changes of GABA+ and Glx in the human brain by using functional  $^1\text{H}$  MEGA-PRESS  
973 MR spectroscopy. *NeuroImage* **105**, 67–75 (2015).
- 974 67. Stagg, C. J., Bachtiar, V. & Johansen-Berg, H. The role of GABA in human motor  
975 learning. *Curr. Biol.* **21**, 480–484 (2011).
- 976 68. Puts, N. A. J., Edden, R. A. E., Evans, C. J., McGlone, F. & McGonigle, D. J. Regionally  
977 Specific Human GABA Concentration Correlates with Tactile Discrimination Thresholds.  
978 *J. Neurosci.* **31**, 16556–16560 (2011).

- 979 69. Scholl, J. *et al.* Excitation and inhibition in anterior cingulate predict use of past  
980 experiences. *eLife* **6**, (2017).
- 981 70. Stagg, C. & Rothman, D. L. *Magnetic Resonance Spectroscopy: Tools for Neuroscience*  
982 *Research and Emerging Clinical Applications*. (Academic Press, 2013).
- 983 71. Jelen, L. A., King, S., Mullins, P. G. & Stone, J. M. Beyond static measures: A review of  
984 functional magnetic resonance spectroscopy and its potential to investigate dynamic  
985 glutamatergic abnormalities in schizophrenia. *J. Psychopharmacol. (Oxf.)* **32**, 497–508  
986 (2018).
- 987 72. Barron, H. C., Garvert, M. M. & Behrens, T. E. J. Repetition suppression: a means to  
988 index neural representations using BOLD? *Philos. Trans. R. Soc. Lond. B. Biol. Sci.* **371**,  
989 (2016).
- 990 73. Andreychenko, A., Boer, V. O., Castro, C. S. A. de, Luijten, P. R. & Klomp, D. W. J.  
991 Efficient spectral editing at 7 T: GABA detection with MEGA-sLASER. *Magn. Reson.*  
992 *Med.* **68**, 1018–1025 (2012).
- 993 74. Govindaraju, V., Young, K. & Maudsley, A. A. Proton NMR chemical shifts and coupling  
994 constants for brain metabolites. *NMR Biomed.* **13**, 129–153 (2000).
- 995 75. Puts, N. A. J. & Edden, R. A. E. In vivo magnetic resonance spectroscopy of GABA: A  
996 methodological review. *Prog. Nucl. Magn. Reson. Spectrosc.* **60**, 29–41 (2012).
- 997 76. Bottomley, P. A. Spatial Localization in NMR Spectroscopy in Vivo. *Ann. N. Y. Acad. Sci.*  
998 **508**, 333–348 (1987).
- 999 77. Mescher, M., Merkle, H., Kirsch, J., Garwood, M. & Gruetter, R. Simultaneous in vivo  
1000 spectral editing and water suppression. *NMR Biomed.* **11**, 266–272 (1998).
- 1001 78. Trabesinger, A. H. & Boesiger, P. Improved selectivity of double quantum coherence  
1002 filtering for the detection of glutathione in the human brain in vivo. *Magn. Reson. Med.*  
1003 **45**, 708–710 (2001).
- 1004 79. Terpstra, M., Marjanska, M., Henry, P.-G., Tkáč, I. & Gruetter, R. Detection of an  
1005 antioxidant profile in the human brain in vivo via double editing with MEGA-PRESS.  
1006 *Magn. Reson. Med.* **56**, 1192–1199 (2006).



- 1007 80. Lin, Y., Stephenson, M. C., Xin, L., Napolitano, A. & Morris, P. G. Investigating the  
1008 Metabolic Changes due to Visual Stimulation using Functional Proton Magnetic  
1009 Resonance Spectroscopy at 7 T. *J. Cereb. Blood Flow Metab.* **32**, 1484–1495 (2012).
- 1010 81. Robertson, C. E., Ratai, E.-M. & Kanwisher, N. Reduced GABAergic Action in the  
1011 Autistic Brain. *Curr. Biol.* **26**, 80–85 (2016).
- 1012 82. Taylor, R. *et al.* Functional magnetic resonance spectroscopy of glutamate in  
1013 schizophrenia and major depressive disorder: anterior cingulate activity during a color-  
1014 word Stroop task. *Npj Schizophr.* **1**, 1–8 (2015).
- 1015 83. Preston, A. R. & Eichenbaum, H. Interplay of hippocampus and prefrontal cortex in  
1016 memory. *Curr. Biol.* **23**, R764–R773 (2013).
- 1017 84. Brogden, W. J. Sensory pre-conditioning. *J. Exp. Psychol.* **25**, 323–332 (1939).
- 1018 85. Brink, W. M. & Webb, A. G. High Permittivity Pads Reduce Specific Absorption Rate ,  
1019 Improve B1 Homogeneity, and Increase Contrast-to-Noise Ratio for Functional Cardiac  
1020 MRI at 3 T. *Magn. Reson. Med.* **71**, 1632–1640 (2014).
- 1021 86. Hess, A. T., Tisdall, M. D., Andronesi, O. C., Meintjes, E. M. & Van Der Kouwe, A. J. W.  
1022 Real-Time Motion and B0 Corrected Single Voxel Spectroscopy Using Volumetric  
1023 Navigators. *Magn. Reson. Med.* **66**, 314–323 (2011).
- 1024 87. Öz, G. & Tkáč, I. Short-Echo , Single-Shot , Full-Intensity Proton Magnetic Resonance  
1025 Spectroscopy for Neurochemical Profiling at 4 T : Validation in the Cerebellum and  
1026 Brainstem. *Magn. Reson. Med.* **65**, 901–910 (2011).
- 1027 88. Terpstra, M. *et al.* Test-retest reproducibility of neurochemical profiles with short-echo,  
1028 single-voxel MR spectroscopy at 3T and 7T. *Magn. Reson. Med.* **76**, 1083–1091 (2016).
- 1029 89. Provencher, S. W. Estimation of Metabolite Concentrations from Localized in Vivo  
1030 Proton NMR Spectra. *Magn. Reson. Med.* **30**, 672–679 (1993).
- 1031 90. Worsley, K. J. & Friston, K. J. Analysis of fMRI time-series revisited--again. *NeuroImage*  
1032 **2**, 173–181 (1995).
- 1033 91. Mangia, S. *et al.* Sensitivity of single-voxel <sup>1</sup>H-MRS in investigating the metabolism of  
1034 the activated human visual cortex at 7 T. *Magn. Reson. Imaging* **24**, 343–348 (2006).

1035 **Acknowledgements**

1036 We would like to thank Aaron Hess for advice regarding the combined fMRI-fMRS sequence. R.S.K.  
1037 is supported by an EPSRC/MRC-funded studentship (EP/L016052/1). A.S. is supported by a Wellcome  
1038 Trust studentship (203836/Z/16/Z). D.D. is supported by the Biotechnology and Biological Sciences  
1039 Research Council UK (BBSRC UK award BB/N0059TX/1) and the MRC (Programme  
1040 MC\_UU\_12024/3). H.C.B. is supported by the John Fell Oxford University Press Research Fund (Grant  
1041 153/046), a seed grant from the Wellcome Centre for Integrative Neuroimaging, a Junior Research  
1042 Fellowship from Merton College (University of Oxford) and the Medical Research Council (MRC) UK  
1043 (MC\_UU\_12024/3). The Wellcome Centre for Integrative Neuroimaging is supported by core funding  
1044 from the Wellcome Trust (203139/Z/16/Z).

1045  
1046 **Author contributions:** All of the authors contributed to the preparation of the manuscript. R.S.K., A.S.,  
1047 D.D., and H.C.B. designed the study; U.E.E. and I.B.I. developed the combined fMRI-fMRS sequence;  
1048 R.S.K., A.S., U.E.E., and H.C.B. acquired the data; R.S.K., A.S., U.E.E., W.T.C., and H.C.B. analysed  
1049 the data.

1050

1051 **Competing interests**

1052 Authors declare no competing interests.

1053

1054 **Materials & Correspondence**

1055 Correspondence and requests for materials should be addressed to:

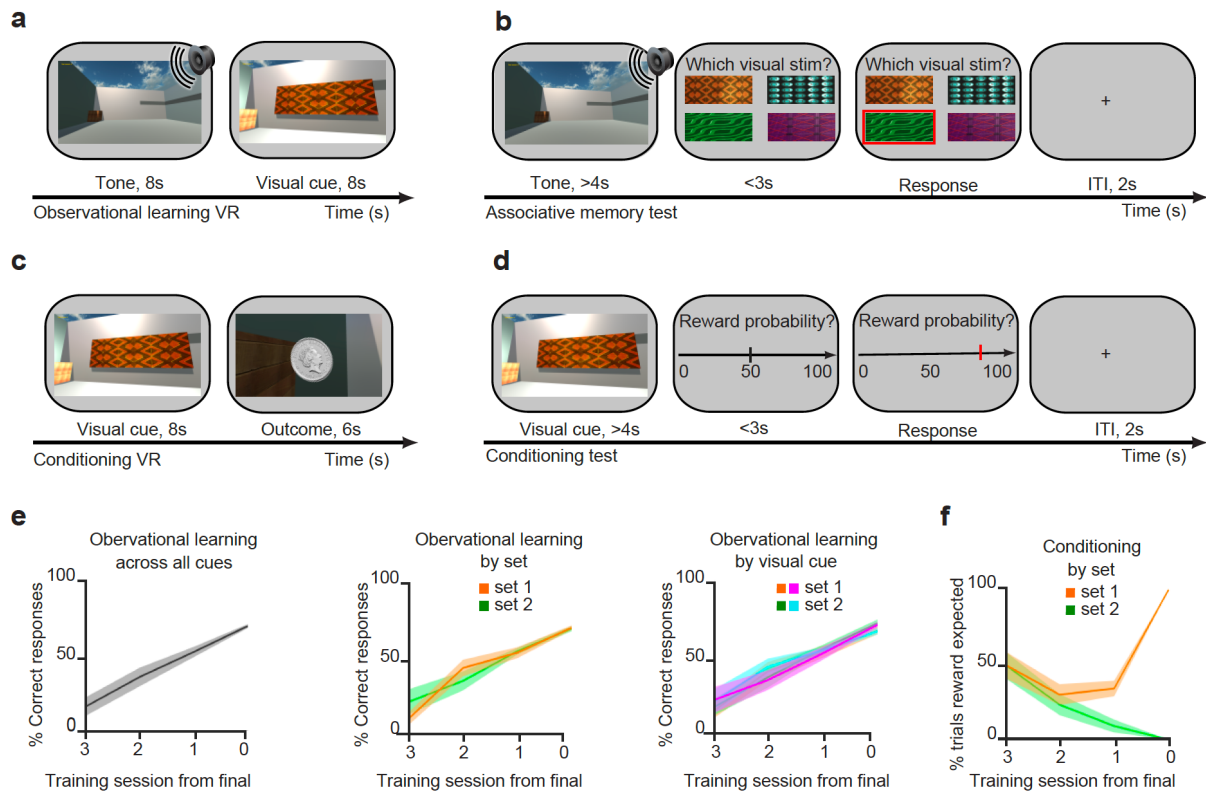
1056 [renee.koolschijn@keble.ox.ac.uk](mailto:renee.koolschijn@keble.ox.ac.uk) and [helen.barron@merton.ox.ac.uk](mailto:helen.barron@merton.ox.ac.uk).

1057 **Supplementary Information**

1058

1059 **Supplementary Figures**

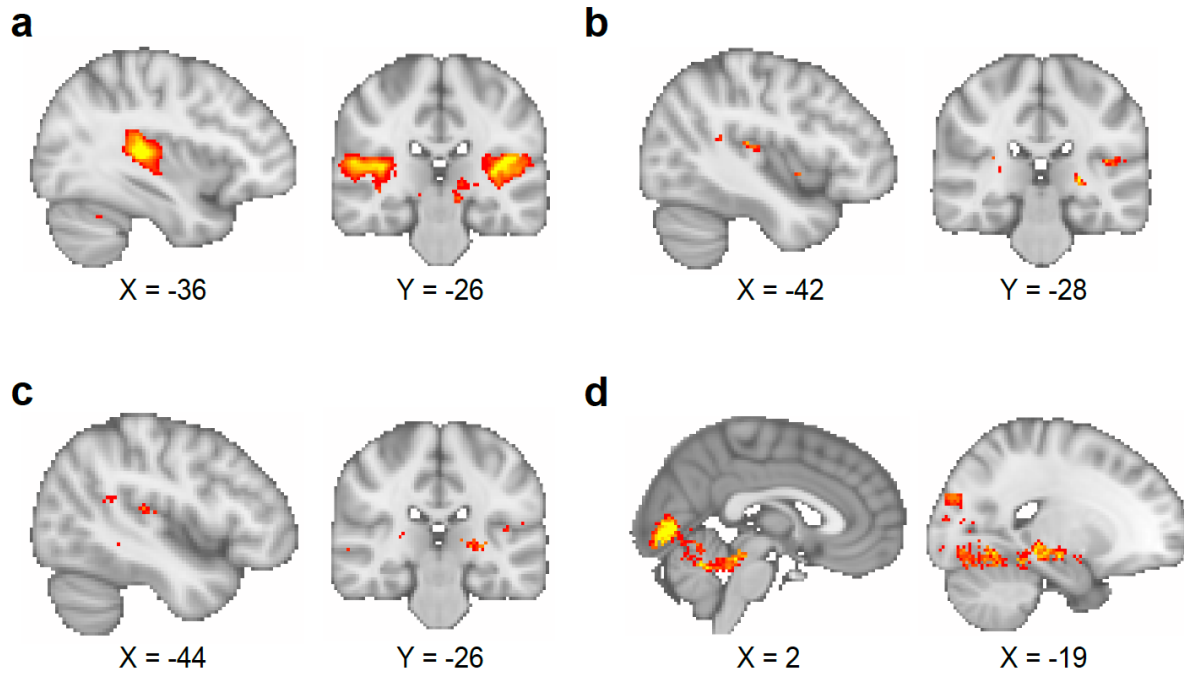
1060



1061

1062 **Supplementary Figure 1 | Behavioural training and performance**

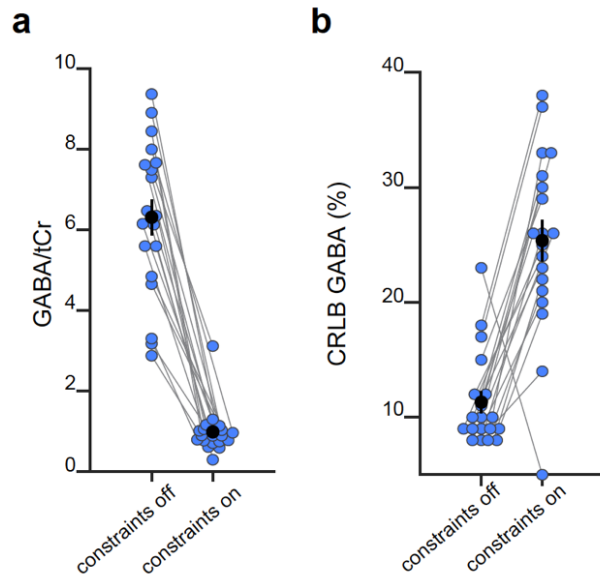
1063 **a-b** On day 1, during the ‘observational learning’ stage, participants learned to associate each of the 80 different auditory cues  
 1064 with one of 4 possible visual cues. **a** The observational learning stage was performed in a VR environment (Fig. 1b). **b** Learning  
 1065 was monitored using an associative memory test, in the absence of feedback. **c-d** On day 2, during the ‘conditioning’ stage,  
 1066 participants learned to associate each of the four visual cues with one of two possible outcomes (monetary reward for set 1;  
 1067 neutral woodchip for set 2) (Fig. 1a). **c** The conditioning stage was performed in a VR environment (Fig. 1b). **d** Learning was  
 1068 monitored using a conditioning test, in the absence of feedback. **e** Left: Participants performed the observational learning task  
 1069 until they showed recall accuracy on the associative memory test of at least 50% of the 80 possible auditory-visual pairs.  
 1070 Middle: On the associative memory test, used to monitor performance during the observational learning, there was no  
 1071 difference in accuracy between auditory-visual pairs in set 1 (rewarded) and set 2 (neutral). Right: On the associative memory  
 1072 test there was no difference in accuracy between auditory cues associated with the four different visual cues. **f** On day 2,  
 1073 participants performed the conditioning task until they reached 100% accuracy on all visual-outcome associations in the  
 1074 conditioning test.



1075  
1076  
1077  
1078  
1079  
1080  
1081  
1082  
1083  
1084  
1085  
1086  
1087  
1088  
1089  
1090  
1091  
1092  
1093  
1094  
1095

**Supplementary Figure 2 | Comparison of different smoothing parameters applied to fMRI data**

**a-c** The BOLD signal response to auditory cues in the inference test was used to assess the effect of different smoothing parameters (contrast of interest: [all trials during inference test – all trials during conditioning]). As noted in the *Methods*, the quality of the fMRI data in the interleaved fMRI-fMRS sequence was compromised relative to contemporary standards for 7T fMRI. The smoothing parameters applied to the data influenced the reliability of the analysis, as illustrated here. **a** Smoothing at the second-level using a 5 mm kernel, approximately two times the voxel size, as recommended<sup>90</sup>, gave significant BOLD signal in bilateral auditory cortex (left auditory cortex,  $t_{17}=8.94$ ,  $p<0.001$ ; right auditory cortex,  $t_{17}=6.76$ ,  $p<0.001$ ; whole-brain FWE corrected; thresholded at  $p<0.001$  uncorrected for visualisation purposes only). This smoothing protocol was used for all analyses presented in the main figures. **b** Smoothing at the first-level using a 5 mm kernel, did not give significant BOLD signal in auditory cortex (whole-brain FWE corrected; thresholded at  $p<0.01$  uncorrected for visualisation purposes only). **c** Smoothing at the first-level using an 8 mm kernel (default for SPM) did not give significant BOLD signal in auditory cortex (whole-brain FWE corrected; thresholded at  $p<0.01$  uncorrected for visualisation purposes only). **d** When contrasting ‘remembered’ and ‘forgotten’ trials in the inference test, smoothing at the first-level using an 8 mm kernel (as in **c**) gave similar results to those presented in Fig. 2c, despite the absence of a main effect response to auditory cues as shown in **c**. Thus, as shown in Fig. 2c, during the question period in the inference test trials (Fig. 1a, d), BOLD signal in the visual cortex and the hippocampus was significantly higher for ‘remembered’ versus ‘forgotten’ auditory cues (‘remembered’ – ‘forgotten’, visual cortex:  $t_{17}=6.01$ ,  $p<0.001$ ; right hippocampus:  $t_{17}=7.58$ ,  $p<0.001$ ; whole-volume FWE-corrected; thresholded at  $p<0.01$  uncorrected for visualisation purposes only).

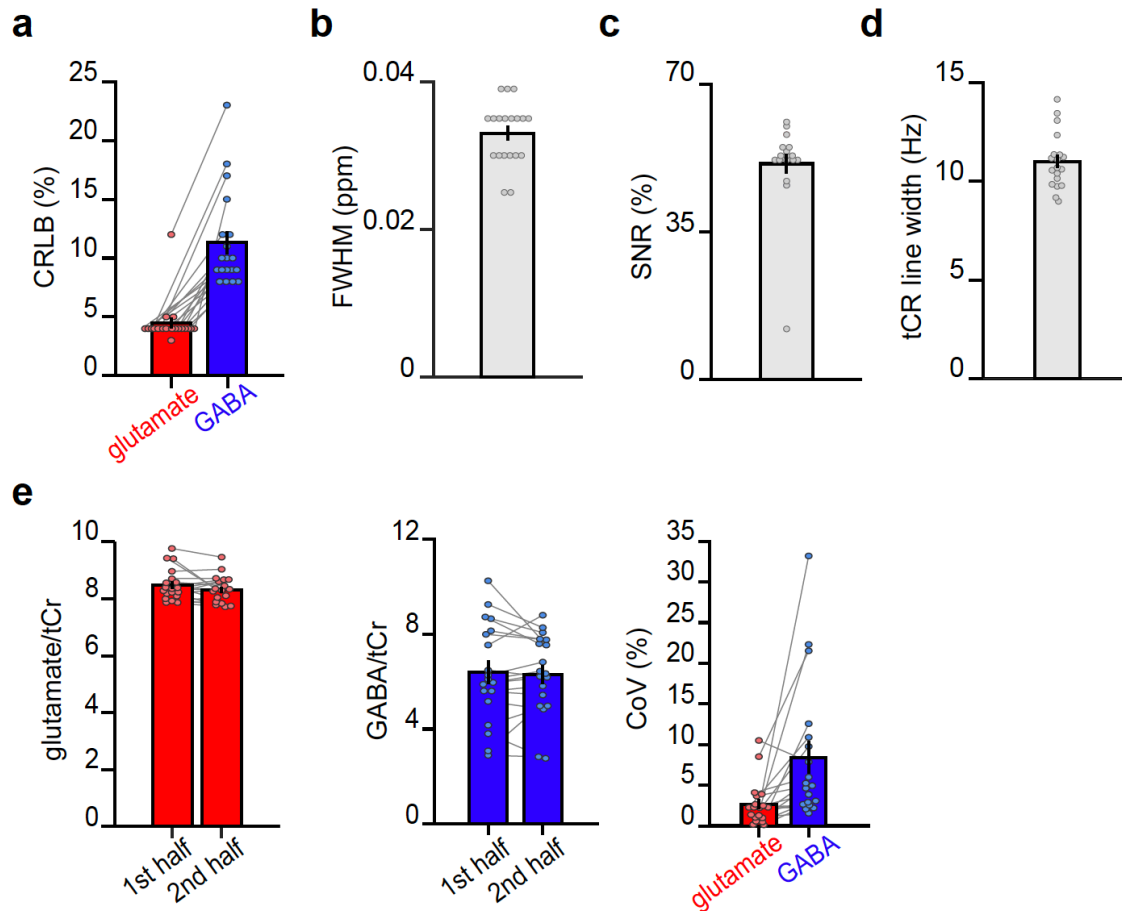


1096  
1097  
1098  
1099  
1100  
1101  
1102  
1103  
1104  
1105  
1106

**Supplementary Figure 3 | Comparison of GABA estimates and uncertainty in the model fit with and without model constraints.**

**a** When using a model fit that constrains metabolite values within a predefined ('physiologically plausible') range (i.e. 'constraints on'), GABA values are reduced together with their dynamic range. However, the assumptions of these constraints are not suitable for detection of dynamic fluctuations in glu/GABA ratio. **b** When using a model fit that constrains the metabolite values within a predefined range, the uncertainty of the GABA estimates increase, as indicated by the Cramér–Rao Lower Bounds (CRLBs). This shows that the reliability of the model fit for GABA is higher when model constraints are removed, namely the approach required to measure dynamic fluctuations in glu/GABA ratio.

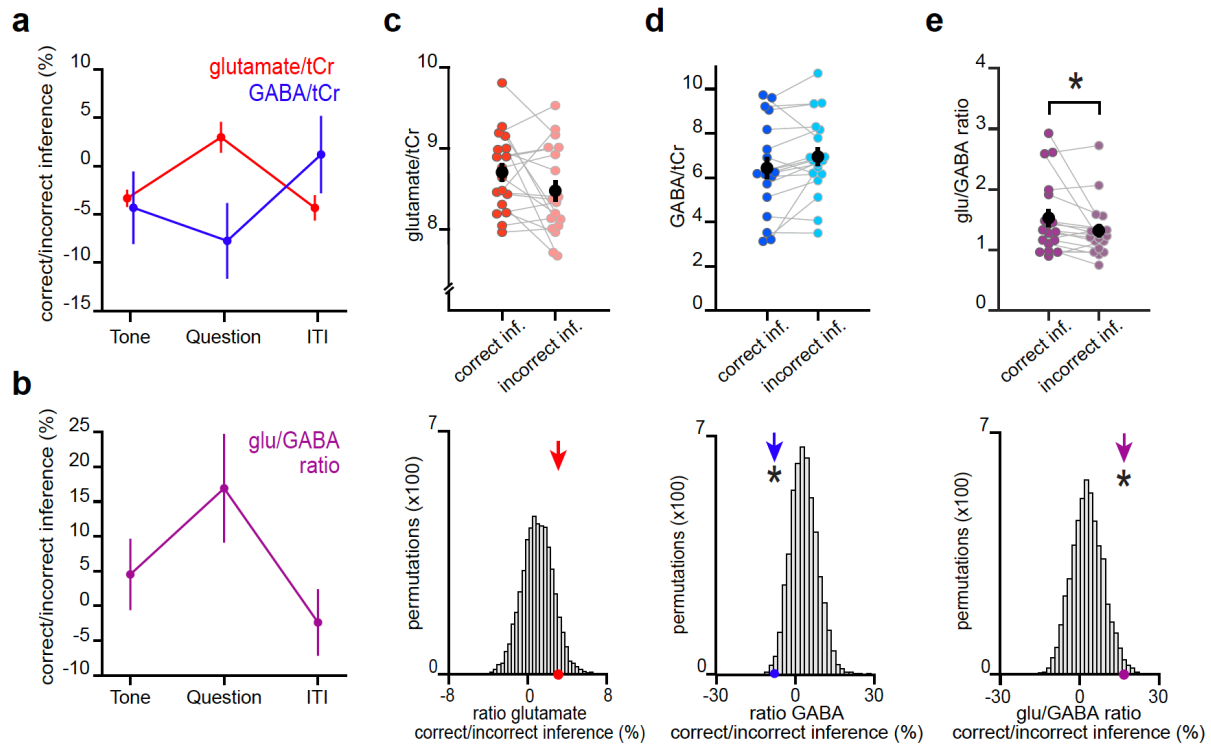
1107



1108  
1109  
1110  
1111  
1112  
1113  
1114  
1115  
1116  
1117  
1118  
1119  
1120  
1121

**Supplementary Figure 4 | MRS data quality metrics across all spectra.**

For each subject, quality metrics across all MRS spectra were assessed (mean total number of spectra: 457). **a** The average Cramér-Rao Lower Bound (CRLB) for glutamate was  $4.47 \pm 0.42\%$  and the average CRLB for GABA was  $11.31 \pm 0.94\%$ . (mean  $\pm$  SEM) **b** The average full width at half max (FWHM) as determined by LCModel was  $0.033 \pm 0.001$  ppm (mean  $\pm$  SEM). **c** The average Signal to Noise Ratio (SNR) as determined by LCModel was  $51.1 \pm 2.37\%$ . (mean  $\pm$  SEM). **d** The average line width of the total Creatine (tCr) peak was estimated to be  $11.01 \pm 0.32$  Hz. (mean  $\pm$  SEM). **e** The intra-subject coefficient of variance (CoV) was estimated by splitting the dataset into two equal halves (on average 278 spectra in each half) and analysing each half in LCModel. We defined CoV as the standard deviation between the 2 halves divided by their mean. The intra-subject CoV for glutamate was  $2.68 \pm 0.62\%$ , and the intra-subject CoV for GABA was  $8.41 \pm 1.96\%$  (mean  $\pm$  SEM). These findings demonstrate stability in our MRS measurements over the course of the scan task. Notably, this analysis differs from standard estimates of intra-subject CoV where test-retest is assessed across two separate scanning sessions.

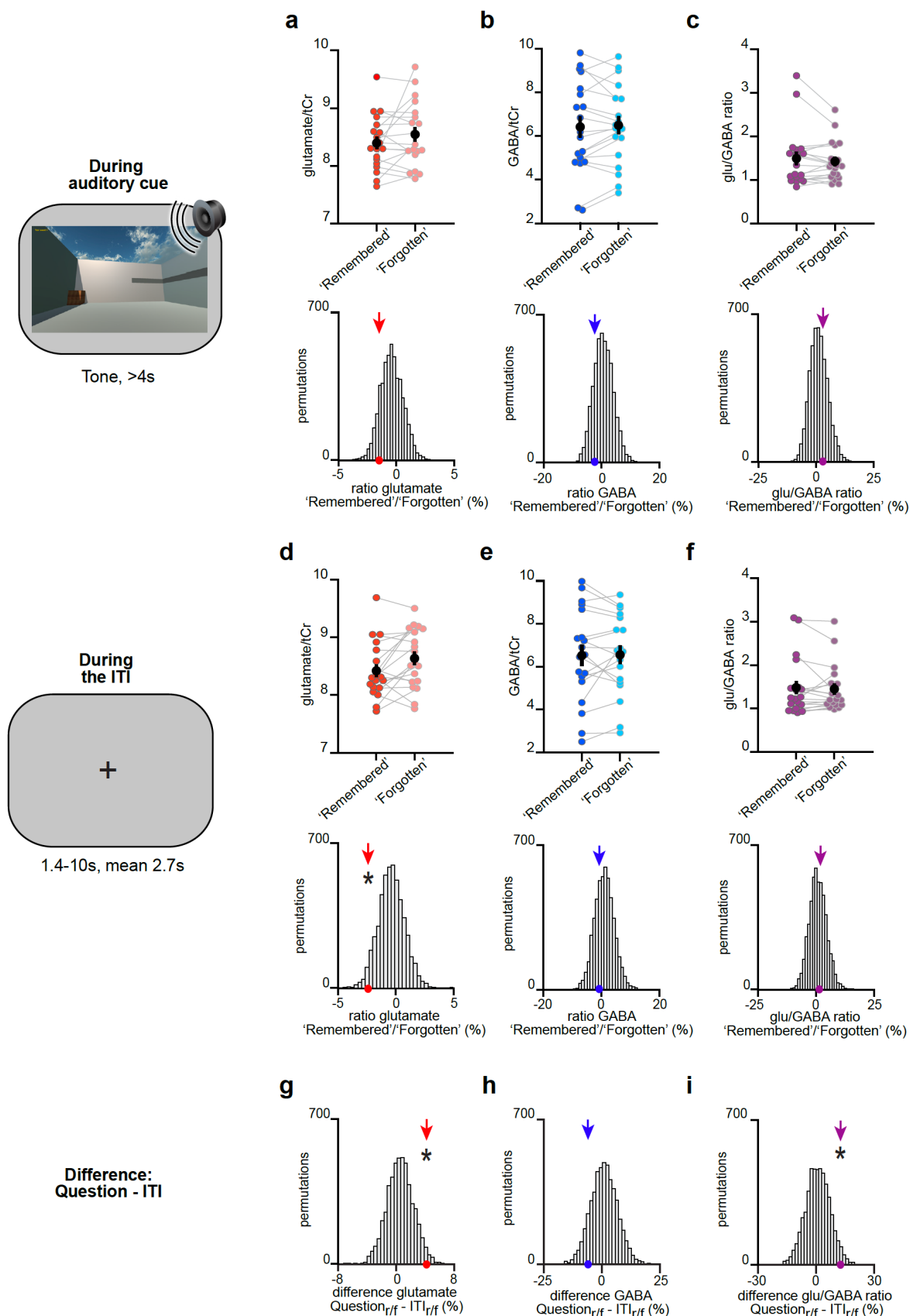


1122  
1123  
1124  
1125  
1126  
1127  
1128  
1129  
1130  
1131  
1132  
1133  
1134  
1135  
1136

**Supplementary Figure 5 | An increase in glu/GABA ratio in V1 during memory recall are also observed when categorising trials into ‘remembered’ and ‘forgotten’ using a less conservative approach**

Here we repeated the analyses in Fig. 3 using only performance on the inference test to categorize trials from the inference test into ‘remembered’ (correct inference) and ‘forgotten’ (incorrect inference). **a-b** Similar to using the more conservative definition for ‘remembered’ and ‘forgotten’ shown in Fig. 3, glu/GABA ratio significantly increased during ‘remembered’ versus ‘forgotten’ trials (‘correct inference’:‘incorrect inference’, glu/GABA ratio:  $t_{17}=2.16$ ,  $p=0.045$ ). This break in glu/GABA ratio was not observed during the ‘tone’ (~7 s) or ‘ITI’ (~2.7 s) periods (‘Tone’, glu/GABA ratio:  $t_{18}=0.88$ ,  $p=0.391$ ; ‘ITI’, glu/GABA ratio:  $t_{18}=-0.50$ ,  $p=0.623$ ). **c-e** Upper row: Metabolite values and glu/GABA ratio during the question period for ‘remembered’ and ‘forgotten’ trials (mean  $\pm$  SEM). Lower row: Comparison of the mean ratio of ‘correct inference’ to ‘incorrect inference’ (coloured arrows) against null distributions generated by permuting the trial labels (x5000) to control for any potential biases in the analyses. Relative to the null distributions, GABA significantly decreased while glu/GABA ratio significantly increased (glutamate:tCr:  $p=0.088$ ; GABA:tCr:  $p=0.017$ ; glu/GABA ratio:  $p=0.011$ ). \* indicates  $p<0.05$ .

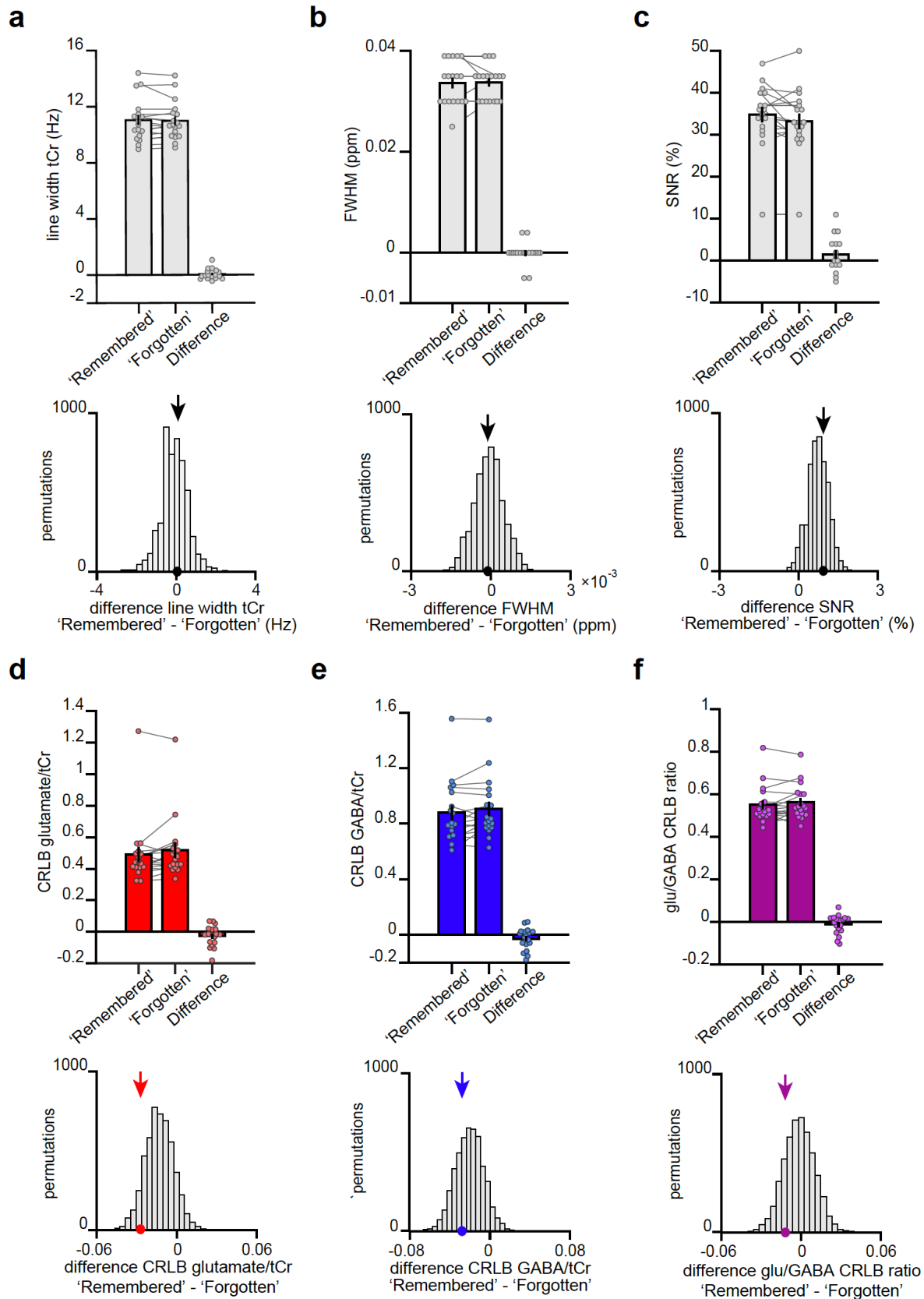




1137  
1138  
1139  
1140  
1141

**Supplementary Figure 6 | The change in glu/GABA ratio is transient and only observed during memory recall**  
a-f Upper rows: The difference in metabolite ratios for 'remembered' versus 'forgotten' trials during the auditory cue period (a-c) and ITI period (d-f) (mean  $\pm$  SEM). Lower rows: To control for any biases due to differences in the number of

1142 'remembered' and 'forgotten' trials, we compared the group mean (coloured arrows) against a null distribution generated by  
1143 permuting the trial labels (x5000). MRS voxel shown in Fig. 2d. **a-c** During the auditory cue period, there was no significant  
1144 increase in glu/GABA ratio between 'remembered' and 'forgotten' trials ('remembered': 'forgotten', glutamate:tCr:  $t_{18}=1.40$ ,  
1145  $p=0.180$ ; GABA:tCr:  $t_{18}=0.80$ ,  $p=0.433$ ; glu/GABA ratio:  $t_{18}=0.74$ ,  $p=0.468$ ). Similarly, there was no significant difference  
1146 between any of the group means and their respective null distributions (glutamate:tCr:  $p=0.107$ ; GABA:tCr:  $p=0.191$ ;  
1147 glu/GABA ratio:  $p=0.314$ ). **d-f** During the ITI period, there was no significant increase in glu/GABA ratio between  
1148 'remembered' and 'forgotten' trials ('remembered': 'forgotten', glutamate:tCr:  $t_{18}=-2.27$ ,  $p=0.040$ ; GABA:tCr:  $t_{18}=0.31$ ,  
1149  $p=0.761$ ; glu/GABA ratio:  $t_{18}=0.31$ ,  $p=0.766$ ). For GABA and glu/GABA ratio, there were no differences between any of the  
1150 group means and their respective null distributions, although a significant decrease was observed for glutamate (glutamate:tCr:  
1151  $p=0.029$ ; GABA:tCr:  $p=0.271$ ; glu/GABA ratio:  $p=0.438$ ). **g-i** To test whether the break in glu/GABA ratio was transient and  
1152 only observed during memory recall, we compared our measure of glu/GABA ratio for 'remembered': 'forgotten' during the  
1153 question period ('Question') to the period immediately after ('ITI') on the same trial. To control for the difference in numbers  
1154 of trials between conditions, we compared the difference of the group means to a permuted null distribution. Compared to the  
1155 respective null distributions, a significant difference was observed for glutamate and glu/GABA ratio between the group means  
1156 for 'Question' versus 'ITI' (glutamate:tCr:  $p=0.021$ ; GABA:tCr:  $p=0.110$ ; glu/GABA ratio:  $p=0.034$ ). 'r/f' indicates  
1157 'remembered': 'forgotten', \*indicates  $p<0.05$ .

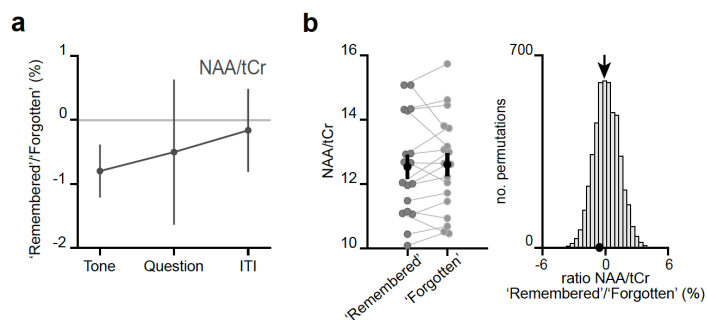


1158  
1159  
1160  
1161  
1162  
1163

**Supplementary Figure 7 | The transient break in glu/GABA ratio observed during recall cannot be explained by changes in data quality metrics or goodness of model fit**

**a-b** At 7T, increases in BOLD effects alter  $T2^*$  of metabolite signals, a phenomenon that results in line narrowing of all signals in the spectrum<sup>91</sup>. This phenomenon is most discernible on the strongest singlets such as total creatine (tCr). To assess the reliability of our fMRS measures we therefore quantified the difference in line width between our conditions of interest. These

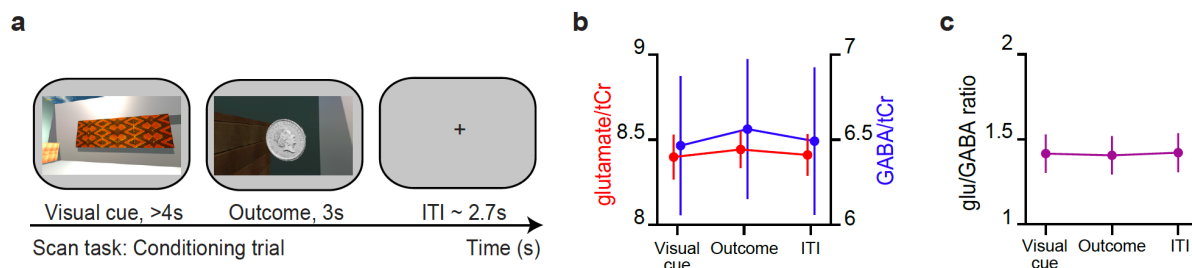
1164 analyses show no significant difference in line width between categories ‘remembered’ and ‘forgotten’. Thus, as linewidth  
1165 was matched across categories there was no evidence for a category-specific bias in BOLD-related confounds for metabolite  
1166 values reported in Fig. 3. **a** The line width of the tCr peak was estimated for each participant for both the ‘remembered’ and  
1167 ‘forgotten’ spectra acquired during the question period of inference test. Across participants we observed no difference in tCr  
1168 line width between our two conditions of interest (‘remembered’ – ‘forgotten’:  $t_{17}=0.61$ ,  $p=0.552$ ) (mean  $\pm$  SEM). To control  
1169 for systematic differences in the number of ‘remembered’ and ‘forgotten’ trials we compared the group mean difference in tCr  
1170 (black arrow) against a null distribution generated by permuting the trial labels (x5000) and re-estimating line width difference  
1171 for ‘remembered’ - ‘forgotten’. Again, there was no significant difference between the group mean difference in tCr and the  
1172 null distribution ( $p=0.403$ ). **b** To further quantify differences in line width for each participant’s ‘remembered’ and ‘forgotten’  
1173 spectra, we compared the full width at half maximum (FWHM). Between our two conditions of interest we observed no  
1174 significant difference in FWHM (‘remembered’ – ‘forgotten’:  $t_{17}=0.21$ ,  $p=0.832$ ) (mean  $\pm$  SEM). There was no significant  
1175 difference between the FWHM group mean for ‘remembered’ – ‘forgotten’ and its null distribution generated as described in  
1176 (a) ( $p=0.467$ ). **c** To verify that the differences between ‘remembered’ and ‘forgotten’ cannot be attributed to a difference in  
1177 signal strength, we assessed the SNR for both conditions. We observed no significant difference in SNR (‘remembered’ -  
1178 ‘forgotten’:  $t_{17}=1.55$ ,  $p=0.140$ ). In addition, there was no significant difference between the SNR group mean difference for  
1179 ‘remembered’ – ‘forgotten’ and its null distribution ( $p=0.312$ ). The positive shift of the null distribution can be explained by  
1180 the difference in number of trials between the ‘remembered’ and ‘forgotten’ conditions (Supplementary Table 5). **d-f** To  
1181 verify that the differences observed between ‘remembered’ and ‘forgotten’ spectra cannot be attributed to differences in model  
1182 fit, we assessed the CRLB for our metabolites of interest. We observed no significant difference in CRLBs (‘remembered’ -  
1183 ‘forgotten’, glutamate:  $t_{17}=-1.73$ ,  $p=0.101$ ; GABA:  $t_{17}=-1.53$ ,  $p=0.145$ ; glu/GABA ratio:  $t_{17}=-1.13$ ,  $p=0.276$ ). In addition, there  
1184 was no significant difference between the CRLB group mean differences for ‘remembered’ – ‘forgotten’ and their respective  
1185 null distributions (glutamate:  $p=0.084$ ; GABA:  $p=0.301$ ; glu/GABA ratio:  $p=0.183$ ). The negative shift of the glutamate and  
1186 GABA CRLB null distributions is related to the difference in SNR between ‘remembered’ and ‘forgotten’; CRLB is lower for  
1187 conditions with higher SNR, indicating a more confident model fit.  
1188



1189  
1190  
1191  
1192  
1193  
1194  
1195  
1196  
1197  
1198  
1199  
1200  
1201  
1202  
1203  
1204  
1205

**Supplementary Figure 8 | The changes in metabolite concentrations cannot be attributed to changes in NAA:tCr**

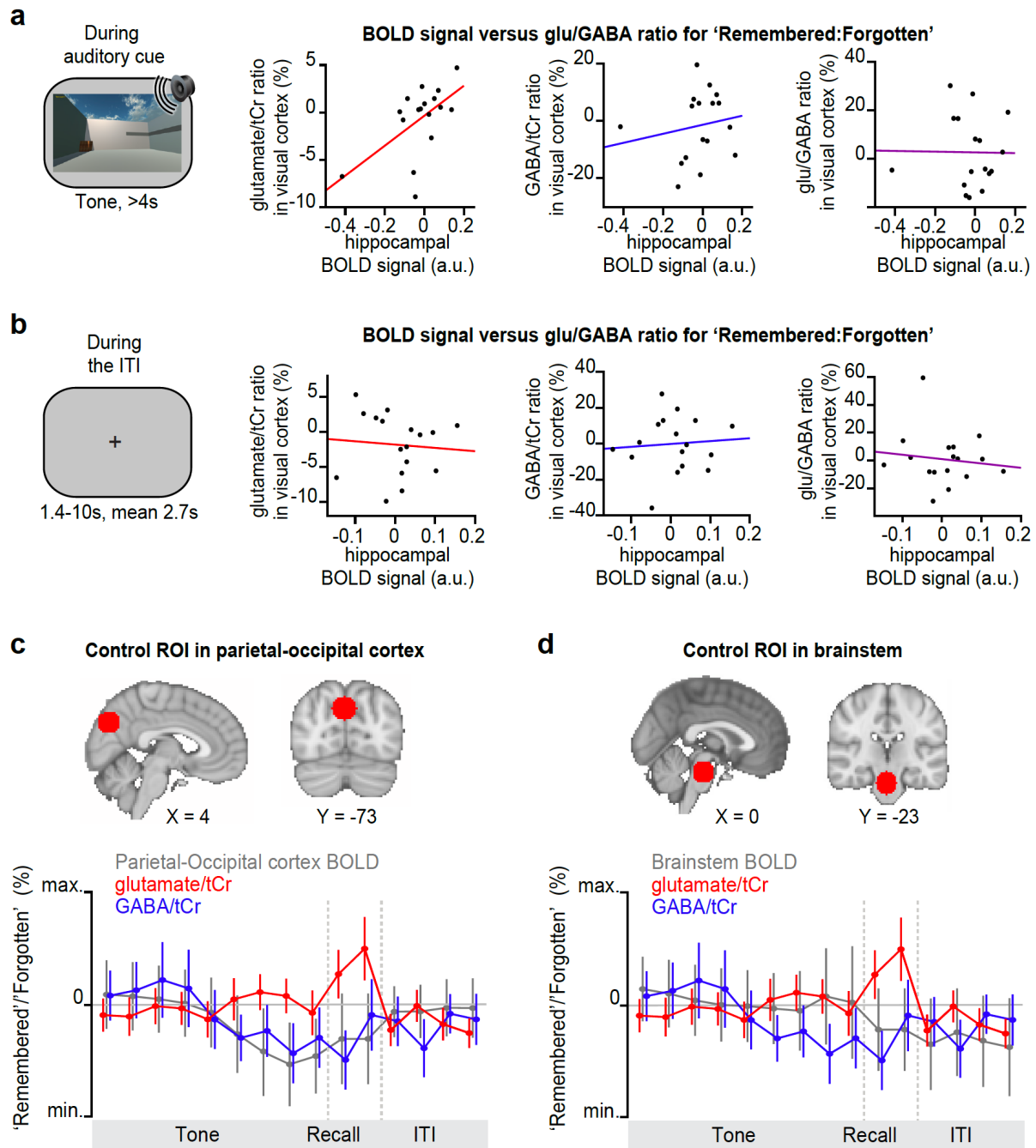
**A** No significant change between 'remembered' and 'forgotten' trials was observed for NAA during the 'Question' period of inference trials (remembered:forgotten NAA:tCr:  $t_{17}=-0.44$ ,  $p=0.663$ ). Notably, NAA has overlapping peaks with GABA but is found at higher concentration. **b** Left: Metabolite values during the question period for 'remembered' and 'forgotten' trials (mean  $\pm$  SEM). Right: Ratios between 'remembered':'forgotten' (black arrows) against null distributions generated by permuting the trial labels. Relative to the null distributions, the mean NAA ratio showed no significant difference (NAA:tCr:  $p=0.259$ ).



**Supplementary Figure 9 | During conditioning trials, no difference in glu/GABA ratio was observed**

**a** Example conditioning trial encountered during the MRI scan task. **b** The concentration of glutamate:tCr and GABA:tCr during the 'visual cue', 'outcome' and 'ITI' periods of conditioning trials. **c** glu/GABA ratio did not change during presentation of the visual cue or outcome, relative to the ITI period ('Visual cue'-'ITI':  $t_{18}=-0.11$ ,  $p=0.915$ ; 'Outcome' - 'ITI':  $t_{18}=-0.21$ ,  $p=0.833$ ).

1206  
1207  
1208  
1209  
1210  
1211  
1212  
1213  
1214  
1215  
1216  
1217  
1218  
1219  
1220  
1221



1222  
1223  
1224  
1225  
1226  
1227  
1228  
1229  
1230  
1231  
1232  
1233  
1234  
1235  
1236  
1237  
1238

**Supplementary Figure 10 | Before and after memory recall, the hippocampal BOLD signal did not positively predict glu/GABA ratio in V1**

**a-b** During 'remembered' relative to 'forgotten' trials on the inference test (the question period, Fig. 1e) we observed a significantly positive correlation between the hippocampal BOLD signal and glu/GABA ratio in visual cortex (Fig. 4b-c). To assess how transient this relationship was, we assessed the relationship between hippocampal BOLD and neocortical glu/GABA ratio during the period immediately before (*a*) and after the question period (*b*). **a** Immediately prior to the question period, during presentation of the auditory cue ('Tone'), the change in hippocampal BOLD signal between subsequently 'remembered' and 'forgotten' trials did not predict the equivalent change in glu/GABA ratio in V1. However, during the auditory cue a positive relationship was observed between the hippocampal BOLD signal and glutamate ratio in V1 (glutamate:tCr:  $r_{16}=0.544$ ,  $p=0.026$ ; GABA:tCr:  $r_{16}=0.28$ ,  $p=0.272$ ; glu/GABA ratio:  $r_{16}=-0.06$ ,  $p=0.809$ ; hippocampal ROI as shown in Fig. 4a). **b** Immediately after the question period, during the inter-trial interval ('ITI'), the change in hippocampal BOLD signal between subsequently remembered and forgotten trials did not predict the equivalent change in glu/GABA ratio in V1 (glutamate:tCr:  $r_{16}=-0.20$ ,  $p=0.444$ ; GABA:tCr:  $r_{16}=-0.04$ ,  $p=0.869$ ; glu/GABA ratio:  $r_{16}=-0.04$ ,  $p=0.876$ ; hippocampal ROI as shown in Fig. 4a). **c-d** Control analyses for Fig. 4d. Upper: ROIs in parietal-occipital cortex (*c*) and brain stem (*d*), defined using a 12 mm sphere. Note: these control regions were restricted to the partial epi volume shown in Fig. 2a. Lower: Moving average showing the ratio of 'remembered' to 'forgotten' trials during the inference test: BOLD signal from parietal-



1239 occipital cortex (*c*, range [-10:10]) and brain stem (*d*, range [-4:4]) shown in grey (n=19), glutamate:tCr (red, n=19, range [-  
1240 8:8]), GABA:tCr (blue, n=19, range [-15:15]). Each point represents a 2.5s time bin (mean  $\pm$  SEM).

1241 **Supplementary Tables**

1242

1243 **Supplementary Table 1 | The effect of sex on behaviour and on glu/GABA ratio in V1**

1244 Using a GLM, differences in sex (male or female) were regressed onto behavioural  
1245 performance during both the inference test and associative memory test, and onto glu/GABA  
1246 ratio during the question period of the inference test. No significant effect of sex was observed.

1247

Test	T-statistic	p-value
Behavioural performance during the <i>inference test</i> (performed inside MRI scanner)	$t_{17}=0.50$	$p=0.622$
Behavioural performance during the post-scan <i>associative memory test</i>	$t_{17}=0.42$	$p=0.674$
glu/GABA ratio in V1 during the question period in the <i>inference test</i>	$t_{16}=1.64$	$p=0.219$

1248

1249

1250 **Supplementary Table 2 | Number of trials per condition**

1251 The number of trials per condition, reported as mean  $\pm$  SEM.

1252

Categorization criteria	No. of trials per condition	
	'Remembered'	'Forgotten'
Using performance on both the inference test and post-scan memory test: 'correctly inferred & recalled' vs 'incorrectly inferred   not recalled' (see Fig. 2b)	$38.95 \pm 1.56$	$39.32 \pm 1.61$
Using performance on inference test alone: 'correctly inferred' vs 'incorrectly inferred'	$59.74 \pm 1.07$	$18.53 \pm 1.04$
Using performance on post-scan memory test alone: 'recalled' vs 'not recalled'	$42.84 \pm 1.46$	$25.53 \pm 1.51$

1253

1254

1255 **Supplementary Table 3 | fMRI contrast for 'remembered' – 'forgotten'**

1256 The fMRI BOLD signal was assessed for a contrast comparing 'remembered' and 'forgotten'  
1257 trials (Fig. 2b) in the inference test. Brain regions that survived whole-volume correction for  
1258 multiple comparisons are listed ( $p < 0.05$  with whole-brain FWE correction at the cluster-level).

Brain region	P FWE-corr, cluster level	T	Peak coordinate in cluster		
			x	y	z
Left hippocampus	$P=0.017$	4.36	-28	-12	-14
Visual cortex	$P < 0.001$	6.93	-26	-56	-16
Right auditory cortex	$P < 0.001$	5.58	38	-26	16
Left posterior parietal cortex	$P < 0.001$	5.00	-44	-52	22

1259 **Supplementary Table 4 | Inter-subject covariance of glutamate and GABA**

1260 Inter-subject covariances (%) for the key metabolite measurements during the 'Question' period of  
1261 inference trials (presented in Fig. 3c-d).

	glutamate	GABA
‘Remembered’	6.66	33.18
‘Forgotten’	5.77	28.76

1262 **Supplementary Table 5 | Average number of spectra (NEX)**

1263 The number of spectra contributing to metabolite estimates during the various trial periods in the  
 1264 inference test (mean  $\pm$  SEM).  
 1265

	Tone	Question	ITI
‘Remembered’	60.05 $\pm$ 2.73	16.17 $\pm$ 1.08	35.53 $\pm$ 1.76
‘Forgotten’	47.42 $\pm$ 2.23	14.61 $\pm$ 1.21	28.37 $\pm$ 1.49

1266

1267 **Supplementary Table 6 | Covariance between hippocampal BOLD signal and fMRS for**  
 1268 **remembered vs. forgotten**

1269 The relationship between fMRI and fMRS during ‘remembered’ versus ‘forgotten’ trials in the  
 1270 inference test was assessed. To this end, fMRS measures of glu/GABA ratio from V1 for  
 1271 ‘remembered’ – ‘forgotten’ were included as covariates in a group analysis for the equivalent  
 1272 fMRI contrast ( $p < 0.05$  with FWE correction at the cluster-level). The only brain region to  
 1273 survive whole-brain correction for multiple comparisons was the left hippocampus. Thus, the  
 1274 BOLD signal in left hippocampus significantly predicted individual differences in glu/GABA  
 1275 ratio measured from V1 during memory recall.

Brain region	P <sub>FWE-corr, peak level</sub>	T	Coordinate		
			<b>x</b>	<b>y</b>	<b>z</b>
Left hippocampus	P=0.005	11.25	-26	-12	-16

1276